Prestressing Concrete with Shape Memory Alloy Fibers

A Thesis
presented to
the Faculty of California Polytechnic State University,
San Luis Obispo

In partial fulfillment of the requirements for the degree of

Master of Science
In
Civil and Environmental Engineering

by
Skye Mikaella Orvis

June • 2009

Advisor: Daniel C. Jansen

Committee Membership

Title: Prestressing Concrete with Shape Memory Alloy Fibers

Author: Skye Mikaella Orvis

Date Submitted: June 2009

Committee Chair: Daniel C. Jansen, Associate Professor

Committee Member: Garrett Hall, Associate Professor

Committee Member: Eric Kasper, Professor

Abstract

Prestressing Concrete with Shape Memory Alloy Fibers

Skye Mikaella Orvis

Concrete is considerably stronger in compression than it is in tension. When cracks form in concrete members, the flexural stiffness of the member decreases and the deflection increases which increases the overall size of the member. Prestressing concrete remedies this problem by inducing a compressive stress in the concrete thereby reducing the net tension in the member and increasing the load required to crack the member. Traditional prestressing is generally limited to large, straight members. During the last decade, shape memory alloys (SMA) have become more prevalent in engineering and civil engineering applications. The shape memory effect refers to the contraction of the SMA when it is heated to its austenite phase. When a prestrain is induced in the SMA, it can be recovered when it goes through the phase change. Nitinol, a NiTi shape memory alloy was used in this research. Thin, steel cables were also tested to provide a comparison. Two different Nitinol alloys were studied in this research. The alloy M wires were elongated to 8% stain while the alloy X wires were prestrained by the manufacturer. The wires were cast into thin concrete beams and once cured, the beams were heated and a phase change from martensite to austenite occurred in the Nitinol. As a result, the Nitinol contracted and compressed the concrete. The SMA fibers are randomly oriented and allow prestressing to occur along all three axis. This is ideal for thin, curved specimens. Third-point bending tests showed that the SMA fibers prestressed the concrete and upon reheating the cracked specimens, the shape memory effect provides partial crack closure.

Key Words: Shape Memory Alloy (SMA), Prestressed Concrete, Nitinol

Table of Contents

List of Tables

List of Figures

Chapter 1
Introduction

1.1 PURPOSE

This project's objective is to explore the prestressing of thin concrete members using shape memory alloy (SMA) wires. Prestressing has developed over the last century, but it is limited to large scale structural elements in bridges, buildings, and parking garages. One of the main reasons for prestressing concrete is that it reduces or eliminates cracking due to tensile stresses which occur due to externally applied tensile forces or bending moments. As a result, the member is stiffer and the reinforcement is not as exposed to water and other elements which shorten the service life of the member. Traditional prestressed concrete uses steel strands or rods that are typically half an inch in diameter or larger. The tendons are either stretched in long prestressing beds or in special ducts that are cast in the concrete. Both methods are fairly labor intensive. These current techniques are not suitable for adaptation to thin, curved members. The research

conducted in this thesis remedies this problem by casting thin SMA wires into the concrete. After the concrete hardens, the entire sample is heated and the SMA wire contracts, which prestresses the concrete. The traditional approach was also followed using small aircraft cables in a long prestressing bed. The data gathered from this testing allowed for a direct comparison between the common methods of prestressing concrete and the new approach with SMA wires. Using SMA wires to prestress the concrete puts no limit on the size or shape of the member being prestressed.

1.2 SCOPE

The experimental program is divided into two parts. In the first portion, small (4”x 1”x 24”) concrete beams were prestressed using steel aircraft cables. This follows traditional prestressing practices, but on a much smaller scale. Both 3/64 and 1/16 inch diameter cables were used and the force applied to the cables varied from 10 to 240 pounds. The cables were released from the prestressing bed and the forces were transfered to the concrete beams at either the 2^{nd} or 14^{th} day. In the second portion of the experiment, Nitinol wires were used to prestress the concrete. Both straight wires, in a similar configuration to the aircraft cables, and short fibers were used. Different combinations of normal steel fibers and prestressed Nitinol fibers were investigated.

The prestressed and reinforced beams were tested for flexural behavior under third point loading. The load and deflections were measured during testing from which the bending moment and corresponding stress at initial crack and maximum bending moment were determined for each sample. In addition, the compressive strength and

dynamic modulus of elasticity of the concrete were measured, and the shrinkage and creep were directly measured from the sample using embedded screws.

1.3 ORGANIZATION

Chapter 2 provides a brief discussion of the history and background of prestressing, and the history of SMAs and the background of Nitinol is described in depth. The shape memory effect as well as the superelastic effect of Nitinol are broken down and explained at a micro structural level. The chapter concludes with a summary of the research conducted with Nitinol and how it is being used in civil engineering applications.

Chapter 3 describes the material properties of the concrete and reinforcement as well as the testing procedures used in the experiment. The chapter starts by discussing the concrete mix design used for all the samples and the material properties of the concrete along with the tests and equations used to determine them. The material properties of the steel cables used in the first portion of testing along with the steel fibers and the Nitinol wire are described. The chapter includes a brief discussion of prestressing losses and the equations used to calculate them. The prestressing bed, test set-up, and testing procedures are discussed at the end of the charter.

Chapter 4 analyzes the data from both portions of the testing. The chapter begins by outlining the test performed. Then, the bending stress required to crack the samples and the prestressing force in the samples were discussed and compared. Elastic shortening, steel versus Nitinol fibers, and crack closure were also examined.

Finally, Chapter 5 summarizes the analysis of prestressing with SMA wires and reviews the conclusions drawn from the analysis. The chapter concludes with some recommendations for future research using SMA wires and fibers to prestress concrete.

Chapter 2
History and Background

2.1 INTRODUCTION

Understanding how Shape Memory Alloys (SMAs) work on a micro structural level is vital to understand how they are used to prestress concrete. The history and background of prestressing along with SMAs is discussed at the beginning of this chapter. The Shape memory effect and superelastic effect of Nitinol is described in detail. In this research, the shape memory effect along with a phase change in the Nitinol wire was used to prestress concrete. The chapter concludes by describing how SMAs have been tested for uses in civil engineering.

2.2 HISTORY OF PRESTRESSING

The idea of prestressing concrete originated in the late nineteenth century. In 1886, P. H. Jackson patented his idea for tightening steel tie rods in concrete arches. Two years later, C. E. W. Doehring also obtained a patent. Doehring's patent was for prestressing metal

wires in concrete slabs (Naaman 2004). Neither of these first attempts at prestressing could withstand the test of time. During that period, only low grade steel was available. This restricted the amount of stress, and subsequently strain, which was placed on the cables. Creep, shrinkage, and other prestressing losses were large enough to eliminate the small amount of prestressing in the cables, thereby eliminating the prestressing force in the concrete. While a number of people including G. R. Steiner, J. Mandl, and M. Koenen studied the issue of prestressing losses, Eugene Freyssinet found a solution (Naaman 2004).

Eugene Freyssinet, a French engineer, is usually credited with the development of prestressed concrete. He designed and constructed several prestressed concrete bridges in France in the 1940's (Somayaji 2001). His strong understanding of prestressing losses helped him remedy these problems. A prestressing loss is any reduction in the stress applied to the concrete by the prestressing tendon which include losses due to the concrete shrinking, the cable relaxing, along with a variety of other sources discussed later. If the change in length due to the concrete creeping and shrinking exceeds the distance the steel cables stretch, all the prestressing is lost. Therefore, high strength and high elongation steel cables were one of his remedies (Naaman 2004).The high elongation helped counteract the prestressing losses due to the concrete creep and shrinkage. Following Freyssinet's improvements, prestressing concrete became a common construction method and is used world wide today.

2.3 BACKGROUND OF PRESTRESSING

Prestressing is a method of reinforcing concrete which induces permanent internal stresses. Concrete is significantly stronger in compression than in tension. The prestressing forces reduce the amount of tension felt by a member, which in turn reduces cracking and flexure.

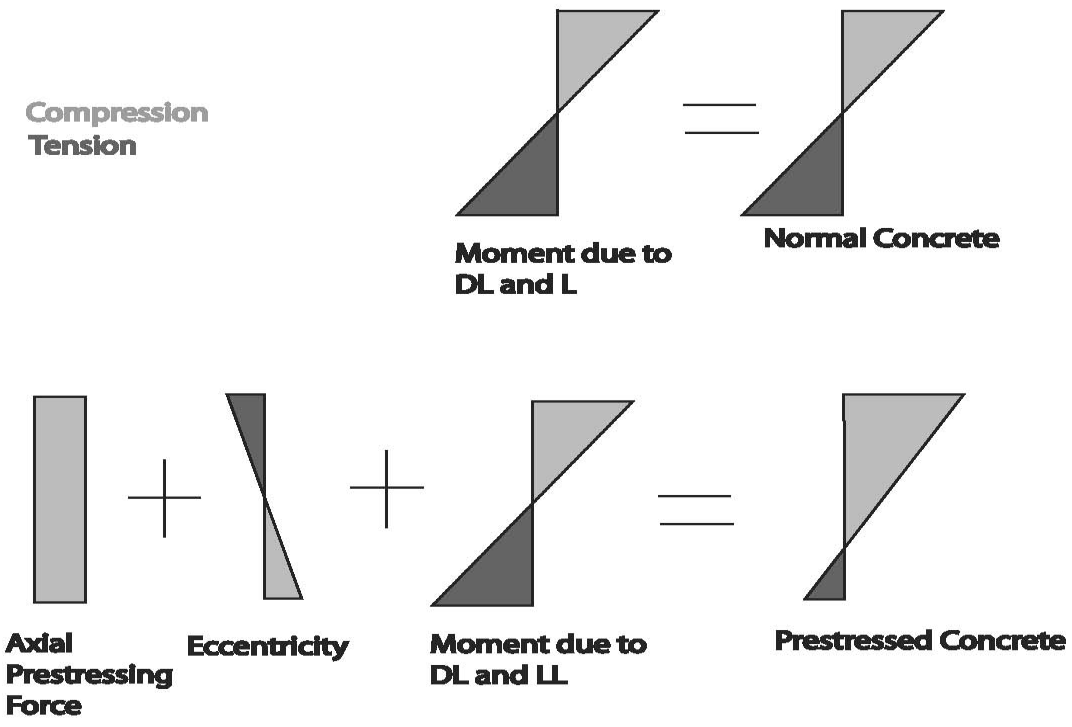

Figure 2.1 - Stresses of Normal and Prestressed Concrete

Prestressing is split into two categories: pretensioned and post-tensioned. The main difference between the two types of prestressing is whether the cables are stressed before or after the concrete is poured.

In pretensioned concrete, the cables are stressed prior to the concrete being poured. It is usually cast in long prestressing beds, which can be as long as 600 ft (Naaman, 2004). The cables are stretched and anchored in beds as shown in

Figure 2.2. The amount of tension applied to each cable is precalculated and specific for each project. The majority of prestressed concrete used today is done with 0.5 or 0.6 inch diameter steel cables. The cables are either low relaxation or stress relieved to help minimize prestressing losses. Concrete is poured around the stretched cables and allowed to set. Most pretensioning plants add accelerators to the concrete to speed up the concrete curing time. This means the members can be removed from the beds earlier and the turn over time on the forms is shortened. Pretensioned concrete is usually removed from the beds when the concrete strength is around 3500 psi. The concrete must be strong enough to withstand the compressive forces induced by the prestressing cables and must have a good bond to the prestressing strand. When the member is being removed from the pretensioning beds, the tendons are released from the frame and the stress is transferred to the member. All of the experiments done in this project will use this technique.

Post-tensioned concrete has ducts cast into the member. After the concrete sets, cables are stretched in the ducts and then anchored to the concrete. Because these

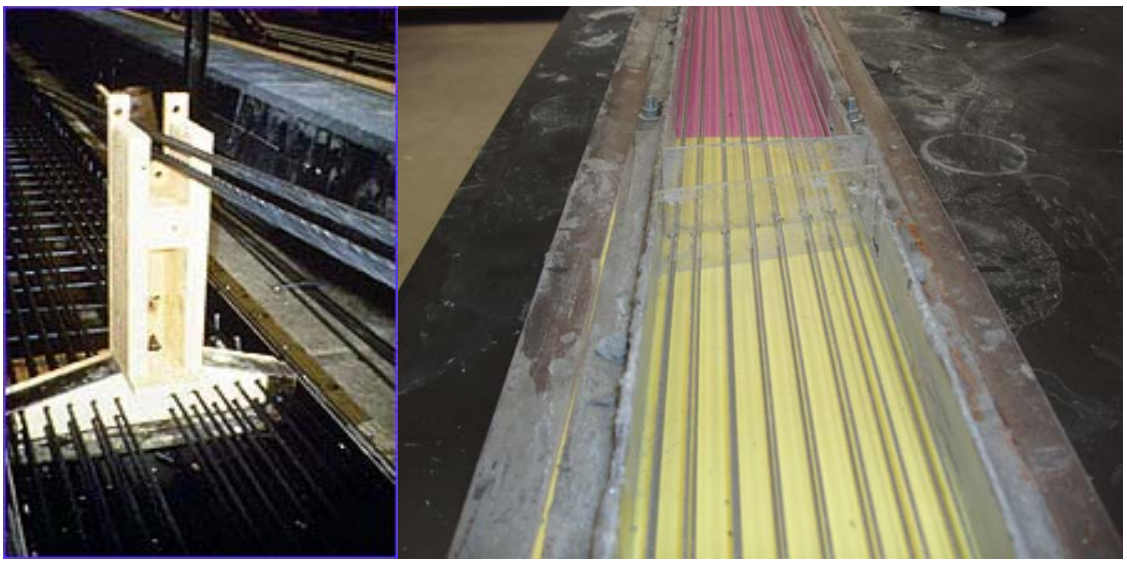

Figure 2.2 - Commercial Prestressing T-beam Bed (left) Source: www.pb.org
Experiment Prestressing Bed (right)

members do not require special forms, accelerators typically are not used and the concrete is allowed to cure for about a week. After the concrete reaches a sufficient strength (around 3500 psi), the cables are stretched, applying stress to the member. Both methods of prestressing produce similar results. The prestressing technique used on a project depends on the type of construction, availability of a prestressing plant, and the design engineer's preference.

2.4 HISTORY OF SHAPE MEMORY ALLOYS

Shape memory alloys (SMA) were discovered and developed during the last century. In 1932, Olander discovered the pseudoelastic behavior of Au-Cd alloy. Six years later, Greninger and Mooradian were conducting experiments with Cu-Zn alloy and observed the formation and disappearance of martensite as a function of temperature. This phase change between austenite and martensite is the key to making the shape memory effect work. Kurdjumov and Khandros along with Chand and Read observed the shape memory effect governed by the thermoelastic behavior of the martensite phase (Fundamental 2000). This phenomenon was widely reported. In the 1960's, Buehler and the U.S. Naval Ordnance Laboratory discovered Nitinol. Nitinol is an equiatomic alloy of nickel and titanium, and the name Nitinol stands for Nickel Titanium Naval Ordnance Laboratory. Following its discovery, many people started studying Nitinol. In the late 1960's and 1970's, Nitinol was used as an implant material and for some medical applications. By the 1980's, orthodontists were experimenting with it. Nitinol's biocompatibility and resistance to corrosion makes it ideal for medical applications. Commercial heart stents made a breakthrough in the mid 1990's (Fundamental 2000). Its superelasticity and shape memory effect make Nitinol a unique alloy that can be used in a variety of applications.

Nitinol can be found in everything from eyeglass frames and cell phone antennas to orthodontic arch wires and undergarment support.

2.5 NITINOL BACKGROUND

Nitinol can be found in three phases: martensite, austenite, and stress-induced martensite. When in the martensite phase, the alloy has a monoclinic crystal structure, $P2_1/m$ (Chen 2001) and is soft and ductile, similar to pewter (Fundamental 2000). When heated, Nitinol converts to the parent structure, austenite, which has an ordered intermetallic crystal structure, B2 or CsCl (Chen et al., 2001). In this phase, the material becomes hard and strong like titanium (Fundamental 2000). The stress-induced martensite is a result of the superelastic effect and has rubber-like characteristics.

The shape memory phase change is based on temperature. A_s is the temperature when austenite starts to form. When the specimen reaches A_f, it has completely changed into austenite when unstrained. M_d is the highest temperature that martensite can form when the sample is under stress. Similarly, as Nitinol cools down, M_s is the temperature when martensite begins to form. Once the sample cools below M_f, it is completely martensite (see Figure 2.3). The nickel-titanium composition and heat treatment have a

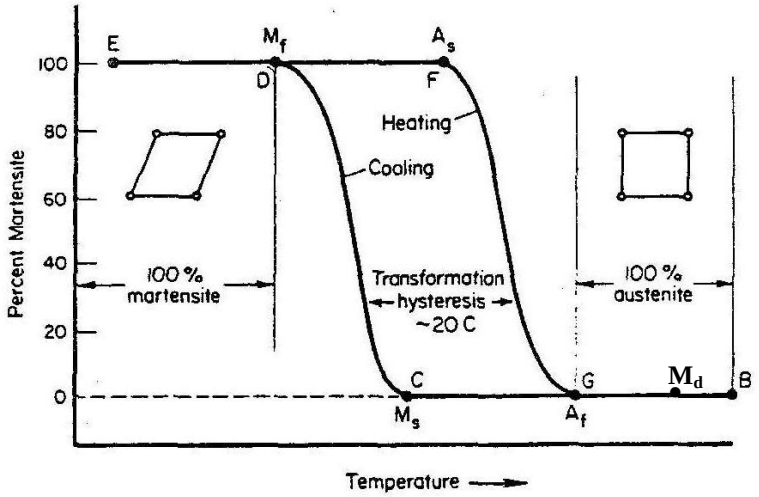

Figure 2.3 - Nitinol Transition Temperatures Source: (Krstulovic-Opara 2000)

large effect on the transition temperatures. A one percent shift in the ratio of nickel to titanium can change A_f by 100 degrees Celsius (Pelton et al., 2003). Similarly, heat treatments can precipitate out or mix back in some of the nickel and change A_f. The maximum stress can also be varied with heat treatments.

As seen in Figure 2.3, the change in crystal structure is a function of temperature. There are three main types of SMA classifications based on width and position of temperature hysteresis based on ambient temperature, shown below in Figure 2.4. Type one is austenite at room temperature and is generally used for the superelastic properties of the SMA. Type two is martensite at room temperature and type three can be either martensite or austenite at room temperature. To prestress concrete either type two or type three SMA transition temperatures are required for the shape memory effect.

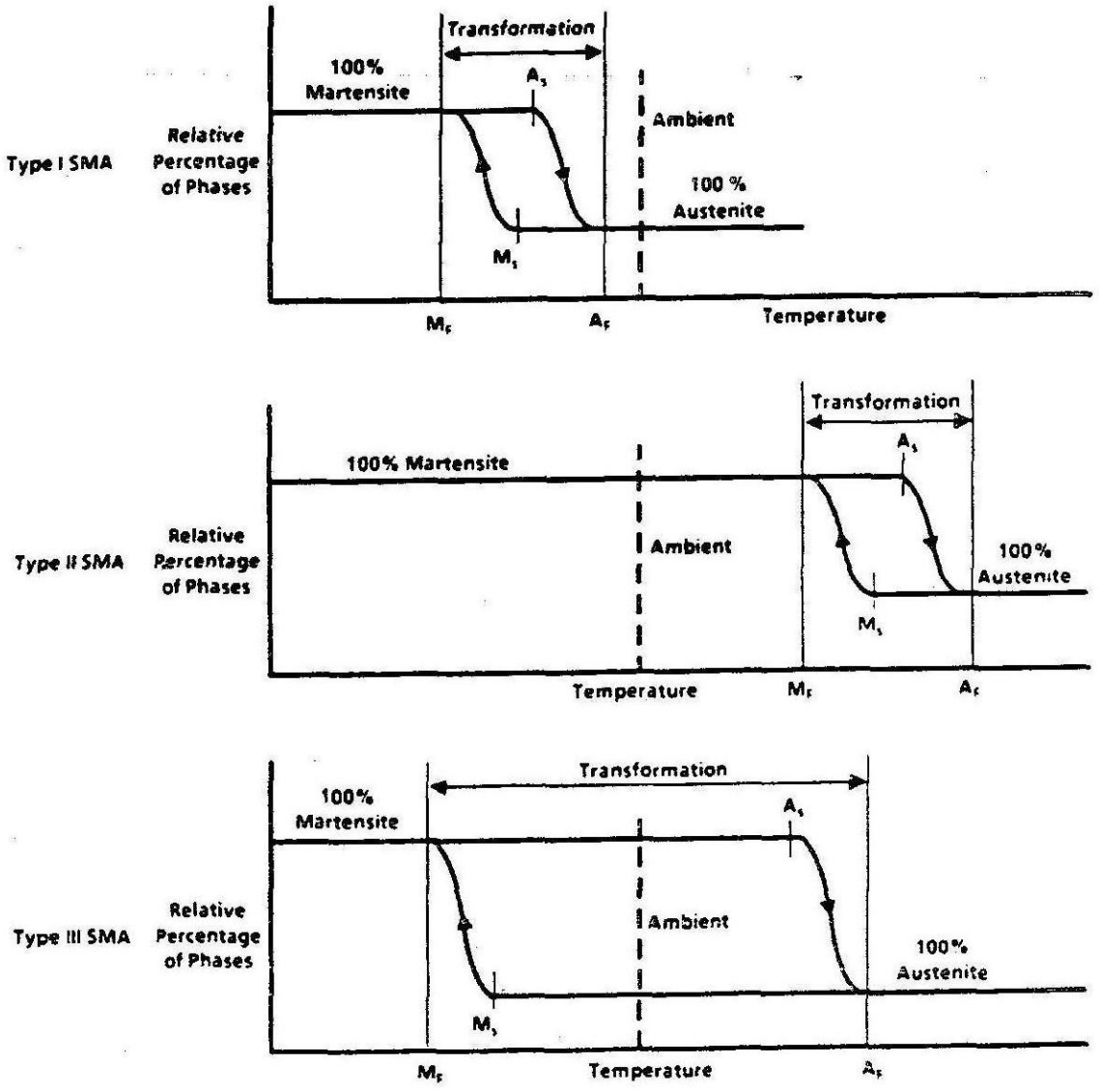

Figure 2.4 - SMA Classifications Source: (Krstulovic-Opara 2000)

2.5.1 Shape Memory Effect

2.5.1.1 Using Shape Memory Effect to Prestress Concrete

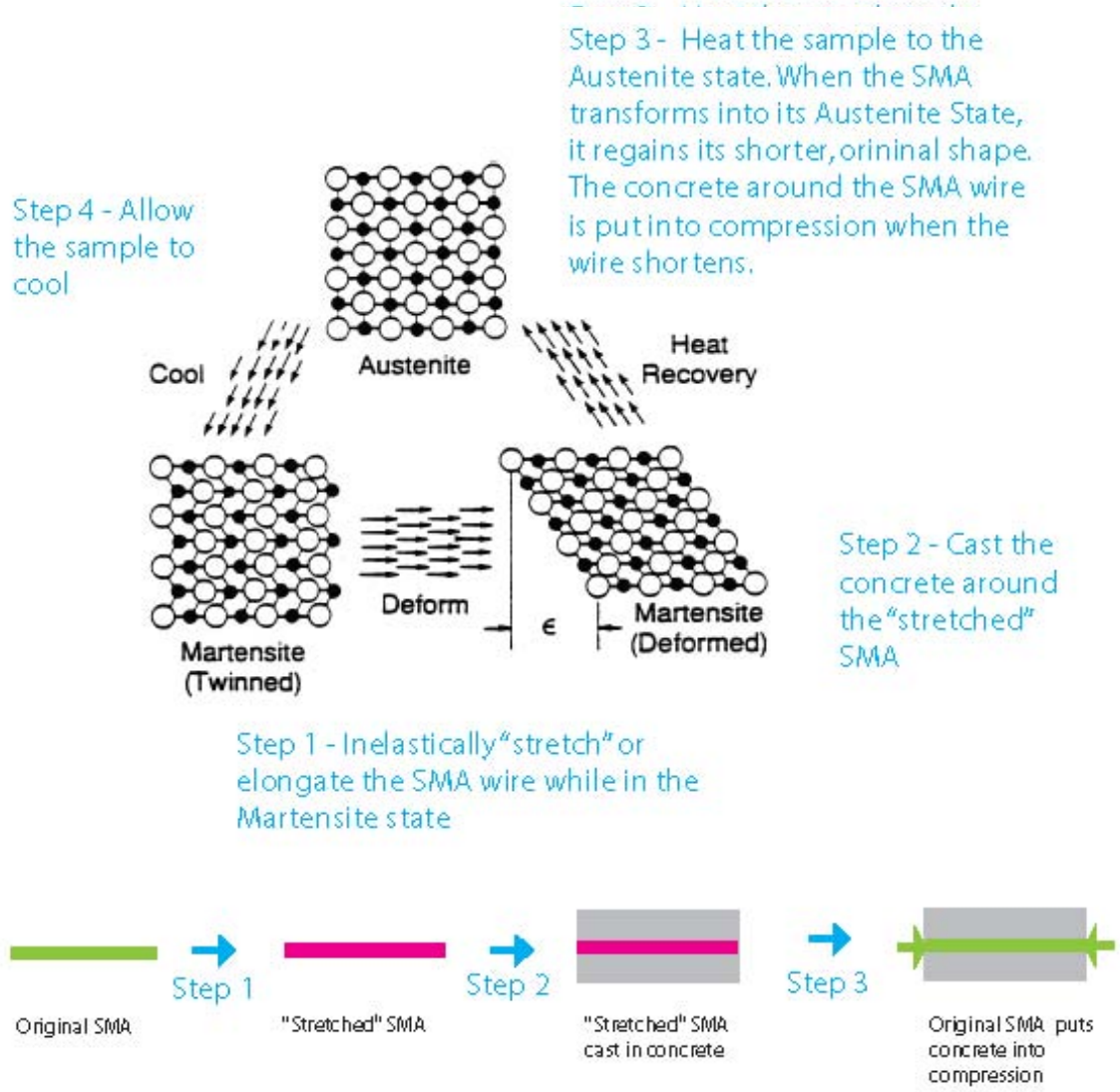

Figure 2.5 - Nitinol Crystal Structure Phase Changes

The shape memory effect is used to prestress concrete. When heated to its austenite phase, Nitinol only has one austenite orientation as seen in Figure 2.5. This is the minimum energy state at a given temperature and stress level. When below M_f, there are 24 possible crystalographically-equivalent habit planes of martensite (Chen 2001). Martensite is easily deformed by twinning. It responds to stress by simply changing the

orientation of its crystal structure through movement of twin boundaries; in other metals slip or dislocation movement occurs. When the crystal structure can no longer change, classic plastic deformation by slip occurs and cannot be completely recovered.

To prestress concrete, the Nitinol wire is first prestrained. The wire in the martensite phase is stretched and twinning occurs as it deforms. Deng et al. (2003) found that the maximum amount of prestraining that can be recovered is 8.1 percent. Later, Deng et al. (2006) reconfirmed this as shown in Figure 2.6. Concrete is then cast around the prestrained Nitinol. After the concrete reaches at least 3500 psi, the entire sample is heated above A_f, transforming the Nitinol into its austenite phase. Then as it cools, depending on its transition temperatures, it can return to its original martensite shape before it was prestrained or remain austenite. The original shape of the wire was shorter,

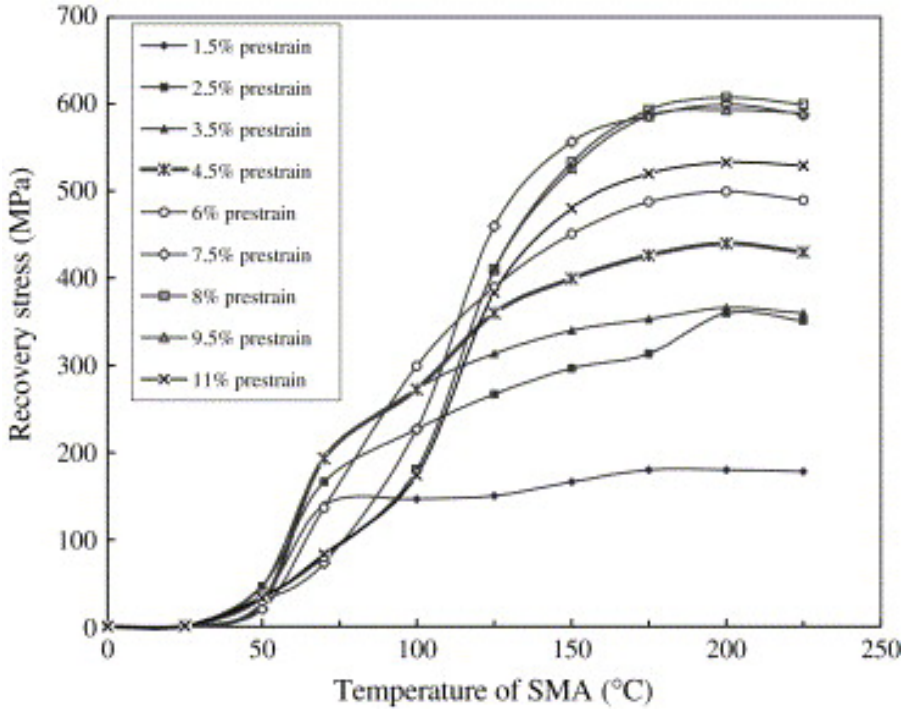

Figure 2.6 - Maximum Recovered Prestrain Source: (Deng et al. 2006)

so as the wire tries to contract, it compresses the concrete (see Figure 2.5). If a type three alloy is used, the sample would remain austenite when it cools, and will transfer the compressive force of both the phase change and the prestraining. This results in a greater prestressing force than with a similar type two alloy.

2.5.1.2 Other Uses of the Shape Memory Effect

A common use of the shape memory effect today is in robots. A specific type of NiTi alloy is used called Flexinol. It is specially designed for high cycle performance. In the Mars Pathfinder, a thin piece of glass that covers a solar cell is moved by electrically heating a Flexinol wire. When either Nitinol or Flexinol is heated, it contracts up to ten percent of its original length, but the total volume remains constant (Nitinol 2007). Nitinol is meant for low cycle or one time use, as it is considerably less expensive than Flexinol.

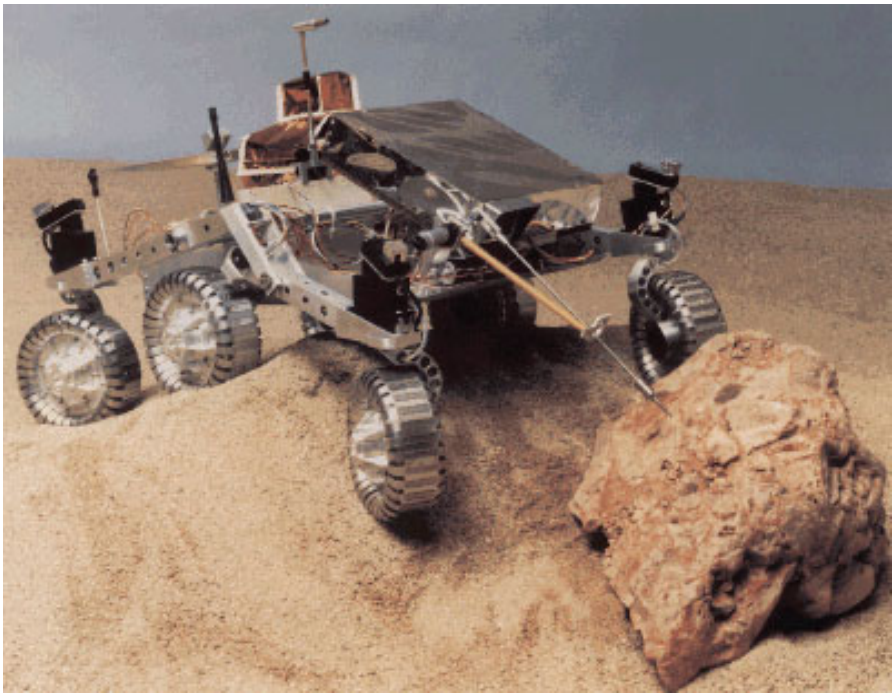

Figure 2.7 - Sojourner, the Mars Pathfinder's mobile robot that landed on Mars (Photo: NASA)

2.5.2 Superelastic Effect of Nitinol

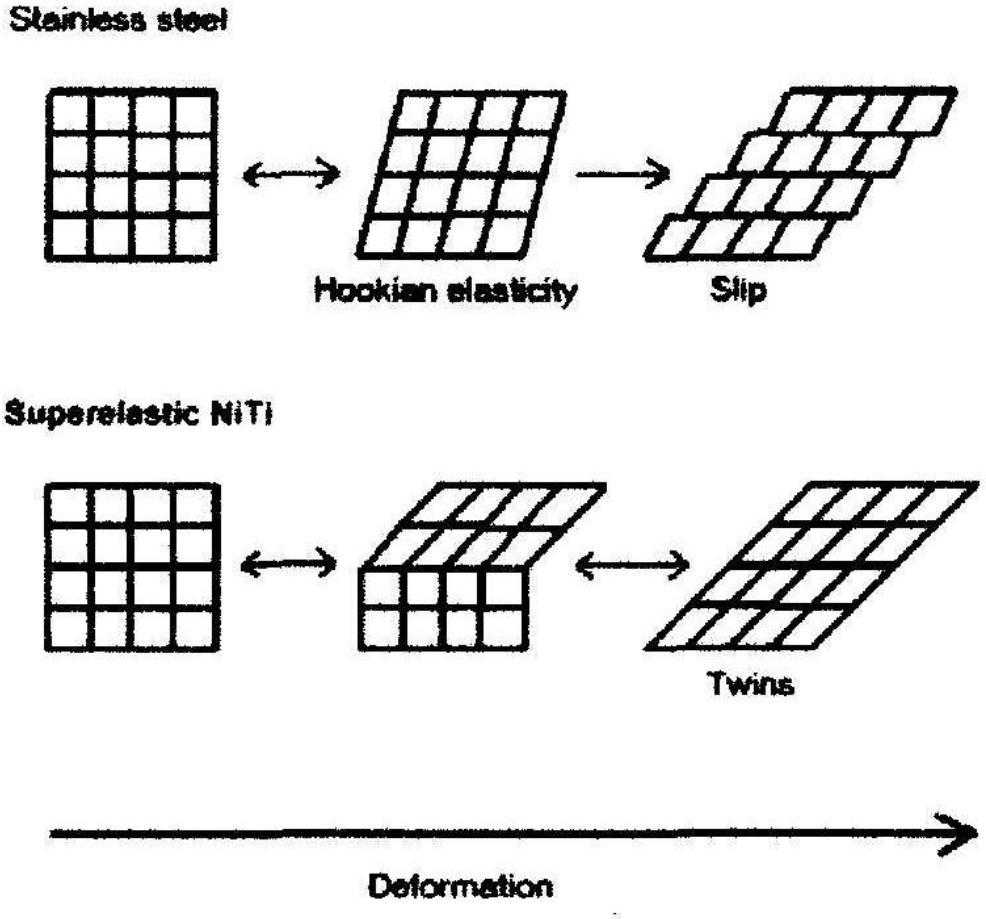

Figure 2.8 – Superelastic Effect Source: (Fundamental 2000)

When stress is applied to Nitinol in the austenite phase, variants form parallel to the direction of the stress and create martensite (Chen 2001). When the stress is removed, the material returns to its austenite structure, which is the reason it is called superelastic. This phase change is stress induced, not temperature induced. In this research, we won't be exploiting the superelastic properties of Nitinol.

2.6 USES OF NITINOL FOR PRESTRESSING CONCRETE

Over the last decade, numerous people have studied the use of Nitinol in civil engineering projects. Smart bridges, actively controlled beams, and base isolation systems have been experimented with. Maji and Negret (1998) concluded that prestressing with SMA, in addition to prestressing with regular prestressing steel, could offset prestressing losses after prolonged use or increase capacity of a bridge on an as needed basis using the two-way shape memory effect. Their test specimens were electrically heated during the testing. They also looked at the bond between the SMA and the concrete. Twisting four wires together resulted in much higher bond strength than an individual SMA wire.

Deng et al. (2006) experimented with actively controlling beam deflection using SMA strands. The wires can be electrically heated and used as actuators to vary the deflection in the beam. They found that four small wires produce more deflection than two large ones. Li et al. (2007) created smart beams by embedding SMA bundles along with traditional prestressing steel cables. If these beams were used in bridges, sensors would detect approaching trucks and turn on an electric current which would activate the SMA bundles and add additional prestressing to the bridge when needed. Pan and Cho (2007) experimented with using small SMA wires as dampers. Over the last few years, many people have researched smart bridges and structures that can sense oncoming traffic or seismic activity and adjust their properties to compensate or counteract the forces.

Hsu (1996) studied the use of SMA to repair, retrofit, or upgrade infrastructure systems. The SMA can self repair beams after earthquakes, explosions, and temporary

overloads by reheating the damaged section. Hsu found that after a beam is loaded to failure, the SMA can restore the beams integrity, correct deflections, and close cracks. The SMA also more than doubles the beam's service load capacity and increases the ultimate flexural strength by about sixty percent. In this experiment, crack closure will be explored by reheating the cracked samples.

Saiidi et al. (2007) studied concrete beams reinforced with SMA bars. The beams were not loaded to failure and they were externally reinforced to save the SMA. They were using the SMA for its superelastic properties and found that the SMA was not very stiff, but had substantially less residual displacement.

The practice of prestressing concrete with SMA has developed as people have researched it and expanded ideas. Krstulovic and Naaman (2000) recognized three limitations of traditional prestressing: limits to the size and shape of the member, high friction losses, and the fact that it is labor intensive. With SMA, the level of prestressing can be changed throughout the life of the structure without the use of jacks or other mechanical devices. Krstulovic and Naaman prestressed small beams with straight SMA wires with the ends of the wires were crimped to improve anchorage. The SMA was prestrained by the manufacturer and they achieved stresses between 50,000 and 85,000 psi in the SMA wire. Their entire specimens were heated in an oven. Deng et al. (2003) also researched prestraining SMA wires; they found that the maximum amount of prestraining that can be recovered is 8.1% and that when heated, the force is proportional to the temperature increase between A_s and A_f.

Electrically heating SMA bars and tendons was researched as a method of prestressing concrete. Kotamala (2004) found that SMA increases flexural strength and

he also measured 39 percent prestressing losses. El-Tawil and Ortega-Rosales (2004) prestressed beams with SMA tendons which were heated electrically during testing. They used 15% prestraining. For both of these experiments, the SMA has to be connected to an electric current during testing. This type of reinforcing could be used in smart structures.

Prestressing with SMA fibers has also been studied. Moser et al. (2005) prestressed concrete using short SMA fibers. To improve the bond with such short wires, the wires were wound into star shapes as seen in Figure 2.9. They used five layers of concrete separated with four layers of star SMA fibers. The samples contained 1.2 percent SMA by volume. When the fibers were heated, they produced 122 ksi of stress which was transferred to the concrete because of the geometric anchorage. Based on their experiments, for cementious materials, the temperature should not exceed 95 degrees

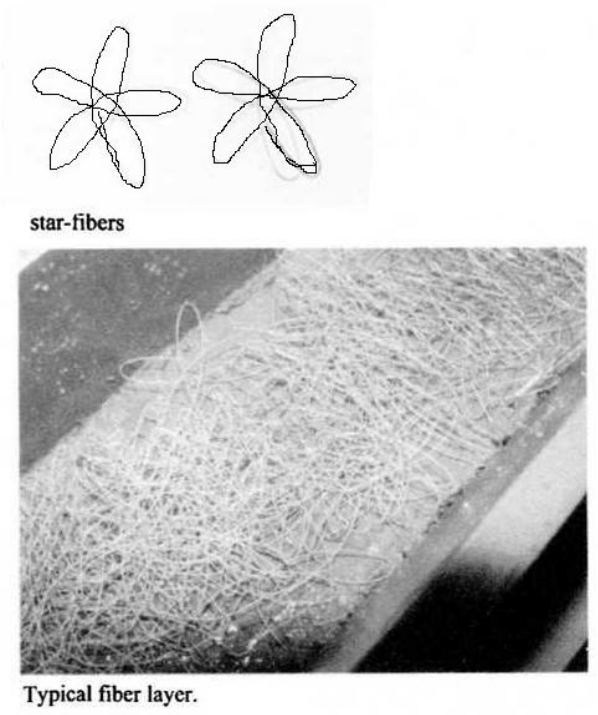

Figure 2.9 – SMA Star Fibers Source: (Moser et al. 2005)

Celsius to avoid thermally induced microcracking in the mortar matrix. Freed et al. (2007) varied the SMA prestressing fibers from zero to two percent by volume and as expected, the breaking stress increased with more fibers. They also concluded that the SMA samples took more stress than with traditionally prestressed samples and that the coefficient of thermal expansion between the concrete and the SMA is negligible. Prestressing with small fibers is ideal for thin walled members and curved objects.

Chapter 3
Material Properties and Testing Procedures

3.1 INTRODUCTION

The material properties of the concrete, steel cables, steel fibers, and Nitinol wire are discussed in this chapter. Numerous theoretical equations as well as experimentally determine equations are defined relating material properties, stresses, strains, and forces. These material properties and equations are used in Chapter 4 to analyze the data obtained from this research. The test setup and loading conditions are outlined also included.

3.2 CONCRETE

The concrete mixture affects the sample in a number of ways. The mixture proportions for this project were designed for both strength and quick curing time. A compressive strength of 3500 psi was set as the minimum 2 day design strength to ensure the concrete will be able to sustain the loads applied by the prestressing cables. The concrete also has

to bond to the cables and be strong enough to hold the cables in place, not letting them slip when released. It also provides a quick turn around time for the prestressing bed to cast more samples. Various material properties are measured to show how the concrete changes with time and the prestressing losses due to the concrete.

3.2.1 Mix Design

A lower water to cement ratio results in high compressive strength. A 0.42 water to cement ratio is required to ensure complete hydration, but a lower water to cement ratio will result in higher strength. In practice, a much higher range of 0.45 to 0.50 is typically used to make the concrete more workable. The concrete mix used has a water to cement ratio of 0.40 along with a 2.5 ratio of sand to type II/V cement. The sand came from the Civil Engineering Department and had a bulk specific gravity of 2.60, absorption of 1.8% and fineness modulus of 2.37. ADVA 500, a high range water reducer or Superplasticizer, produced by GRACE Construction Produces was used to improve workability. It was add to each batch to get the desired consistency.

PolarSet, also produced by GRACE Construction Products, was used to reduce the setting time and produce high early strengths. It is a non-corrosive, non-chloride set accelerating admixture that follows ASTM C 494 (Grace, 2002). The highest typical addition rate of 60 fl oz/100 pounds of cement was chosen because it produced the strongest 2 days strength.

Table 3.1 – Concrete Mix

Component	Weight (g)
Sand	2000
Cement	800
Water	339
ADVA	2.5
PS	30

3.3 MATERIAL PROPERTIES

3.3.1 Concrete Material Properties

3.3.1.1 Compressive Strength

While concrete always continues to gain strength, it typically gains over half of its strength in the first seven days and the majority of its strength in twenty eight days. Most of the samples were demolded and tested after two days. The design two-day concrete strength is between 3500 and 4000 psi. to ensure that the concrete can withstand the compressive stresses induced by the prestressing tendons. Seven and fourteen day tests were also be conducted when the sample's compressive strength was around 5000 psi and 5500 psi, respectively. Three by six cylinders were used for the majority of the testing. Figure 3.1 shows how the compressive strength of three by six cylinders compares to four by eight cylinders of the same concrete mix and resulted in the correlation:

$$f'_{c4x8} = 0.831\left(f'_{c3x6}\right) \qquad \text{(Eq. 3.1)}$$

Where: f'_{c4x8} = Compressive Strength of 4x8 Cylinder

f'_{c3x6} = Compressive Strength of 3x6 Cylinder

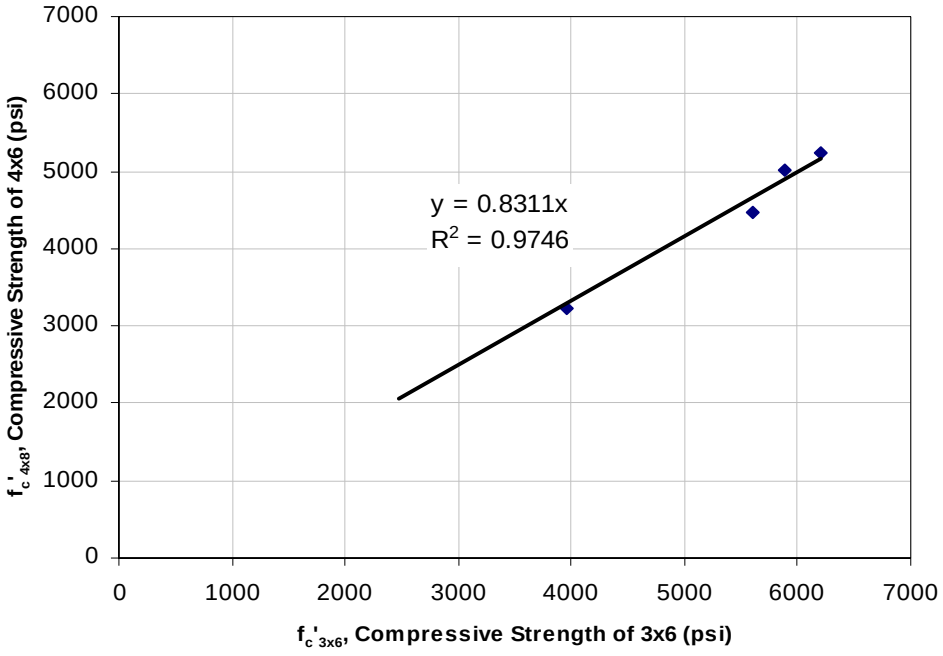

Figure 3.1 – Correlation Between Compressive Strengths of 3x6 and 4x8 Cylinders

This relationship is slightly lower then the relationship suggested by Neville (1956). When Neville compared relative concrete strength to cylinder diameter, he found that four by eight cylinders crush at around about 92.6 percent of the compressive strength of three by six cylinders. For the concrete mix used in this experiment, the four by eight cylinders crushed at 83.1 percent of the three by six cylinders' compressive strength.

3.3.1.2 Static Modulus of Elasticity

The static modulus of elasticity of concrete, $E_{C,}$ is required to calculate some of the prestressing losses in the concrete. E_C was determined per ASTM C 469-02, "Standard Test Method for Static Modulus of Elasticity and Poisson's Ratio of Concrete in Compression." Four by eight cylinder samples were compressed to forty percent of their maximum compression strength four times. This test produced a stress-strain curve shown in Figure 3.2 with E_c equaling the average slope of the chords between 0.00005 strains and 0.4 f_c' or 1300 psi. The 28 day strength, $f_c'_{28,}$ was 5250 psi. Figure 3.3 shows how E_C varies as the sample cures.

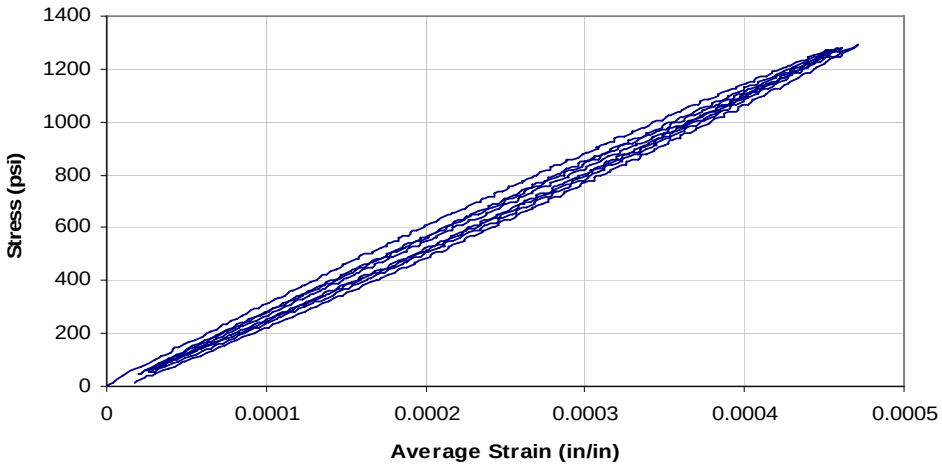

Figure 3.2 – 2 Day Stress-Strain Curve

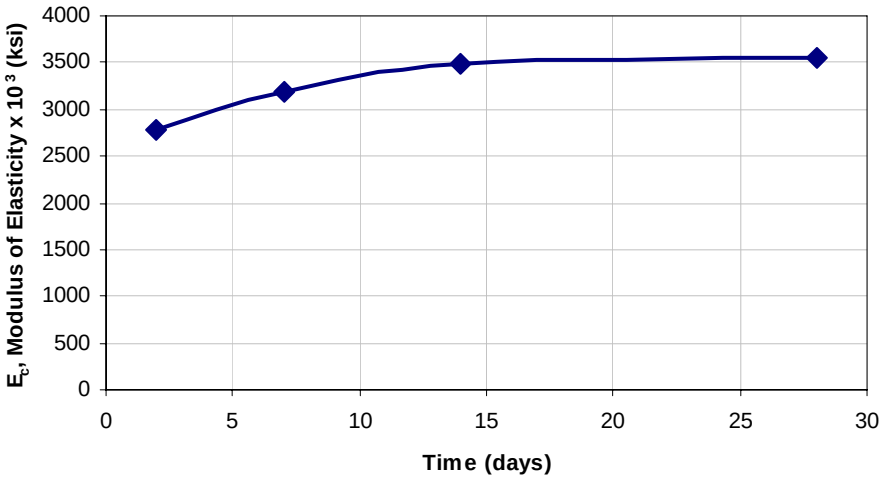

Figure 3.3 – Concrete Static Modulus of Elasticity

3.3.1.3 Dynamic Modulus of Elasticity

The Dynamic Modulus of Elasticity of the concrete was measured following ASTM C 215, "Standard Test Method for Fundamental Transverse, Longitudinal and Torsional Resonant Frequency of Concrete Specimens." For this test, an E-Meter designed by James Instruments Inc. shown in Figure 3.4, was used to find the resonant frequency. The apparatus was arranged for the flexural resonance test with the vibrator located at the center of the specimen and the accelerometer at one of the edges. The test uses the same one by four by twenty four (1"x4"x24") inch samples used later in the third-point bending tests. Per ASTM C215, the dynamic modulus of elasticity, E_D is:

$$E_D = CWn^2 \text{ (psi)} \qquad \text{(Eq. 3.2)}$$

Where: $C = 7.69 \times 10^{-4} L^3T/bt^3$

L = Length of Specimen in inches

T = a correction factor interpolated from ASTM chart ≈1.04

(poisson's ratio = 1/6)

b = width of prism in inches

t = thickness of prism in inches

W = Weight of specimen in pounds

n = frequency of the fundamental mode of flexural vibration in Hz

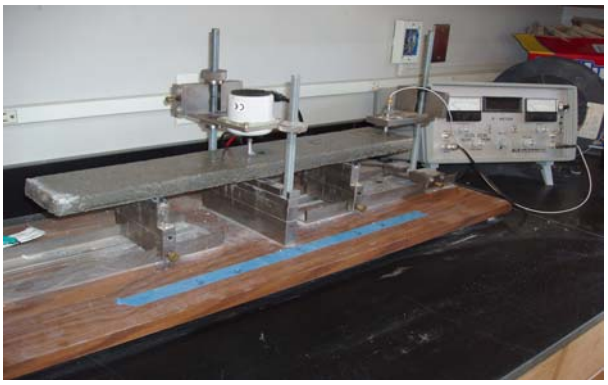

Figure 3.4 - Dynamic Modulus of Elasticity Test

3.3.1.4 Relationship between E_C and E_D

Using the E-meter to test the samples is valuable because it is non-destructive. The dynamic modulus of elasticity can be measured on the actual test specimens then related back to the static modulus of elasticity using:

$$E_C = 0.83(E_D) \quad \text{(Eq. 3.3)}$$

Where: E_D = Dynamic Modulus of Elasticity

E_C = Static Modulus of Elasticity

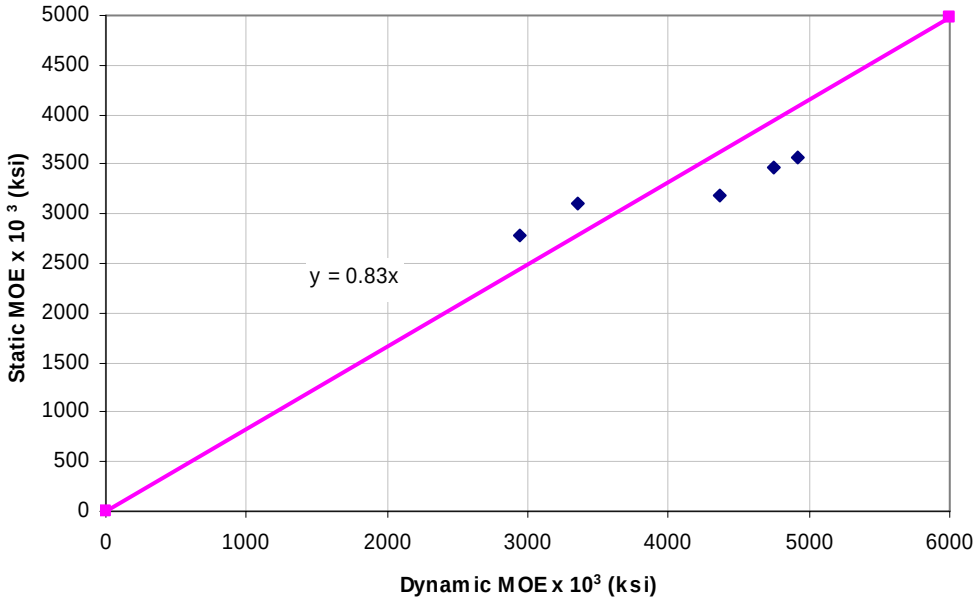

Figure 3.5 – Dynamic vs. Static Modulus of Elasticity

Of the many equations used to predict this relationship, the simplest one, developed by Lydon and Balendran, fit the data points the best (see Figure 3.5).

3.3.1.5 Modulus of Rupture

The modulus of rupture was determined using a third-point loading test. Because concrete is much stronger in compression, an unreinforced specimen in a flexure test will fail in tension. A vertical flexure crack will form near the section with the largest moment. Based on the load applied, the tensile strength can be calculated. For a rectangular cross section under third point loading:

$$MOR = \frac{PL}{bt^2} \qquad \text{(Eq. 3.4)}$$

Where: MOR = Modulus of Rupture in psi

P = load in pounds

L = length in inches

b = width in inches

t = thickness in inches

According to ACI, the theoretical modulus of rupture equals:

$$MOR = 7.5\, f_c'^{0.5} \qquad \text{(Eq. 3.5)}$$

Where: f_c' = compressive strength on concrete

For this research, as shown in Figure 3.6, the modulus of rupture follows the experimentally derived equation:

$$MOR = 0.275\, f_c'^{0.89} \qquad \text{(Eq. 3.6)}$$

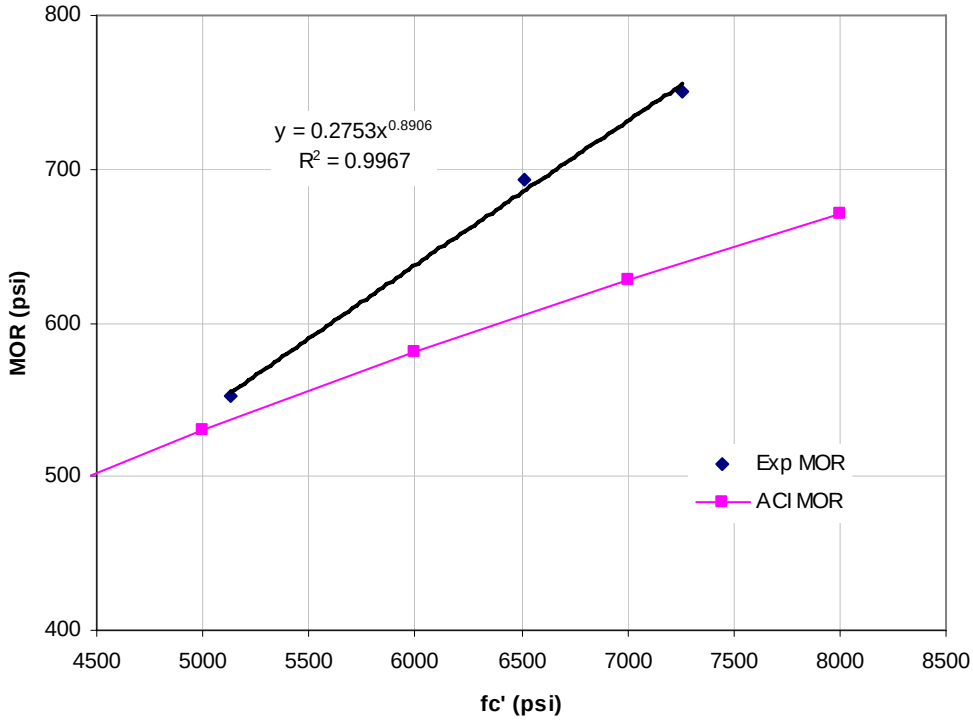

Figure 3.6 – Concrete Modulus of Rupture

This equation is used for all the theoretical calculations.

3.3.1.6 Theoretical Initial Crack

The theoretical force required to crack a prestressed sample was calculated using the modulus of rupture and the prestressing force applied to the sample. Because the concrete is prestressed by either the steel cables or the Nitinol wire, the load required to crack the sample in tension increases. For a rectangular cross section under third-point loading, the force required to crack a sample, corresponding to the modulus of rupture, is:

$$P_{cr} = MOR + \frac{Fd}{L} \qquad \text{(Eq. 3.7a)}$$

Where: P_{cr} = cracking load in pounds
MOR = modulus of rupture in psi
F = prestressing force in psi
L = length in inches
d = height in inches

This equation can also be rearranged in order to determine the prestressing force if the load required to crack the sample is known and assuming the measured value of the modulus of rupture:

$$F = \left(\frac{P_{cr} L}{bd^2} - MOR \right) \left(bd^2 \right) \qquad \text{(Eq. 3.7b)}$$

The bending stress in the sample before it cracks under third-point loading equals:

$$\sigma = \frac{PL}{bd^2} \qquad \text{(Eq. 3.8)}$$

Where: σ = bending stress in psi

3.3.2 Steel Cable Material Properties

Aircraft cables were used in the first stage. Two different sizes of cable were used: 1/16 inch diameter and 3/64 inch diameter. The material properties of the steel are summarized below:

Table 3.2 – Steel Material Properties Summary

Diameter (in)	1/16"	3/64"
Area (in^2)	1.02E-03	6.39E-04
Ultimate Tensile Strength (lbs)	478	285
Ultimate Tensile Stress (ksi)	468	446
Modulus of Elasticity (psi)	44.4E+06	54.2E+06

3.3.2.1 Steel Tensile Strength

The ultimate tensile strength of the steel cables was determined experimentally. Three cables of each size were stretched until failure as seen in Figure 3.7. There average breaking strength was used as the ultimate tensile strength.

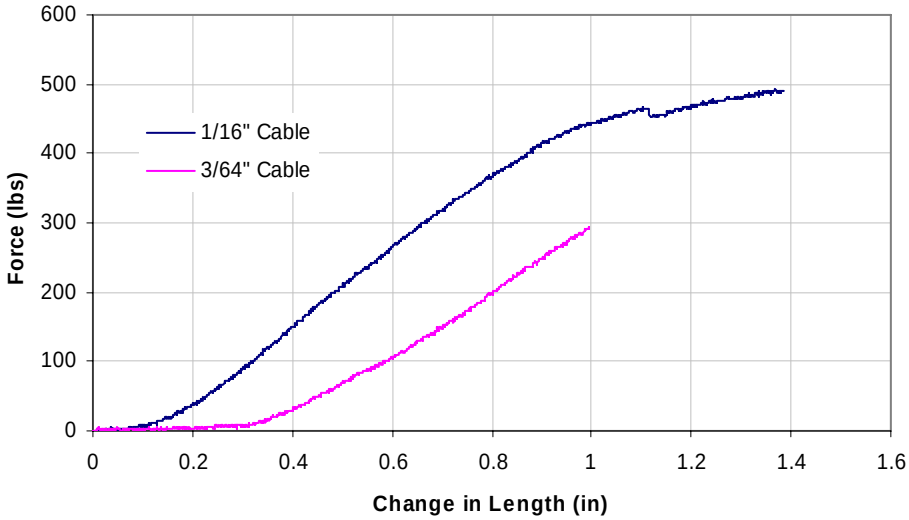

Figure 3.7 – Steel Tensile Strength

3.3.2.2 Steel Modulus of Elasticity

To determine the modulus of elasticity of the steel cables, E_s, two cables of each size were stressed in the prestressing bed. The change in length of the cables was measured with each additional twenty pounds until the force reached 200 pounds. As seen in Figure 3.8, the stress in the cable is plotted against the strain. The slope of the resulting line is the modulus of elasticity, E_s. For the 1/16 inch diameter and 3/64 inch diameter cables, 44.4 x 10^6 psi and 54.2 x 10^6 psi were used as the E_s respectively.

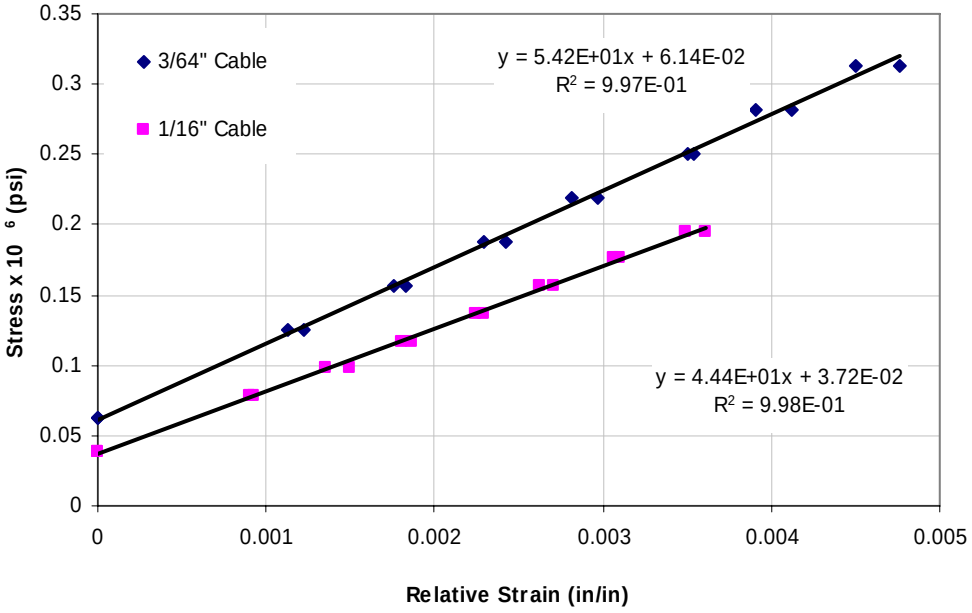

Figure 3.8 – Steel Cable Modulus of Elasticity

3.3.2.3 Steel Pull-out Tests

Bondage between the concrete and the wire is vital for the prestressing force to be transferred into the concrete. If the cable slips under the prestressing load, the prestressing force is lost. To determine the strength of the bond between the concrete and the cable, pull out test were conducted. Steel wires were embedded in concrete at three different depths as seen in Table 3.3. After the concrete cured for two days, the same amount of time before the actual samples were released, the wires were loaded until they either broke or slipped under the load. Pull-out tests were conducted with the 1/16 inch diameter cable and with three strands from the 1/16 inch diameter cable. The 1/16" cable is made of six strands twisted around a center one. Three of these strands were twisted around each other and tested. The maximum prestressing force applied to the 1/16 inch diameter cables was 240 pounds. As seen in Figure 3.9, an embedment depth of just less than two inches is required to ensure the cable does not slip when the cables are released.

Table 3.3 – Steel Cable Pull-out Tests

Wire	Embedment Length (in)	Max. Load (lbs)	Failure Mode
1/16"	6	431.6	Slip
	2	264.8	Slip
	1	119.5	Slip
3 strands	6	205.2	Break
	2	131.2	Slip
	1	66.5	Slip

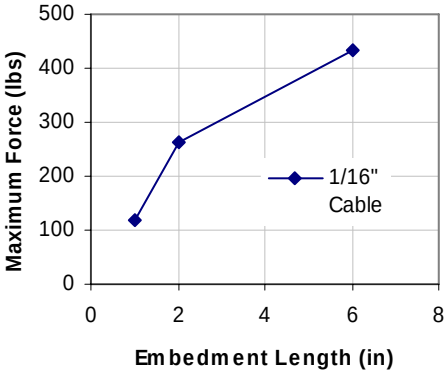

Figure 3.9 – 1/16" Cable Bond Strength

3.3.3 Steel Fiber Material Properties

Steel fiber was tested to provide a comparison to the SMA fiber samples. Samples were made with only steel fiber as well as a blend of steel fibers and SMA fibers. The steel fibers are made by Dramix and they do not provide any prestressing to the sample. As seen in Figure 3.10, the steel fibers are initially stuck together in sheets and are added to the concrete in this form. As they mix with the concrete, the glue dissolves and the individual fibers are dispersed through the concrete. This process also adds a substantial amount of air to the mix. The material properties of the steel fibers are summarized below:

Table 3.4 – Steel Fiber Material Properties Summary

Diameter (in)	0.02
Area (in^2)	$1.26x10^{-3}$
Length (in)	1.41
Material	Low Carbon Steel
Coating	None
Specific Gravity	7.85

Figure 3.10 – Steel Fiber

3.3.4 Nitinol Wire Material Properties

Nitinol wire was used in the second stage. Two different sizes of wire were used: 0.04 inch diameter and 0.074 inch diameter. Each type of Nitinol wire was tested in two configurations. Samples were reinforced with straight wires as seen in Figure 3.12. It was also cut into fibers and hooks were bent into each end as shown in Figure 3.11. A blend of the 0.04 inch diameter wire fibers and plain steel fibers was also tested. The material properties of the nitinol wires are summarized below:

Table 3.5 – Nitinol Material Properties Summary

Diameter (in)	0.04	0.075"
Alloy	M	X
Area (in^2)	0.00126	0.00430
Modulus of Elasticity (psi)	Varies with Temperature 5×10^6 to 11×10^6	
Elongation (%)	17.6	10 Min
Ultimate Tensile Strength (lbs)	~152	149
Ultimate Tensile Stress (ksi)	196	35
Active A_f (ºC)	66.5	150
SMA Classification	Type 2	Type 3

Figure 3.11 – 0.04" SMA Fiber

The A_f, tensile stress, and elongation for the nitinol wire were determined by the manufacturer. The tensile strength was experimentally determined. In the alloy X wire, a brittle failure occurred where the sample was bent around the test machine during the tensile strength test. If overworked when bending the hooks in the alloy X fibers, a brittle failure also occurred.

Figure 3.12 – Straight 0.04" Nitinol Wire

3.3.4.1 Nitinol Pull-out Tests

Because the SMA wires were smooth, pull-out test with different end anchor methods were tested. The end of the wire was tested in a knot configuration and a spiral configuration. A test was also conducted with two wire twisted together. While all of the SMA pull-out tests, shown in Table 3.6, resulted in forces greater then the prestressing force applied by the wire, a hook was selected to anchor the SMA fibers. The straight SMA wires were cast as a continuous wire which ran back and forth in the sample to eliminate ends were the wire could slip.

Table 3.6 – Nitinol Pull-out Tests

Specimen		Max. Load	Failure Mode
.04 SMA	knot	192.2	Break
	spiral	153.3	Break
	twist	178.1	Slip

3.3.4.2 Nitinol Prestraining

To prestrain the 0.04 inch SMA wire, the wire was first tested to determine the yield point. Figure 3.13 shows that the SMA begins to strain harden around 50 pounds, and it fails around 152 pounds. If the maximum prestressing force results from 8 percent prestraining, the prestraining force to achieve maximum prestressing should be around 58 pounds. The wire was then tested at different prestraining forces. The wires were prestrained, then held at a fixed distance and heated. The samples were allowed to cool and the force remaining in the wire is the prestressing force as shown in Figure 3.14. To achieve the maximum prestressing force, a prestraining force between 58 and 60 pounds was used. The wire was prestrained in 35 foot pieces, then cut into fibers or bent into 19 inch straight pieces.

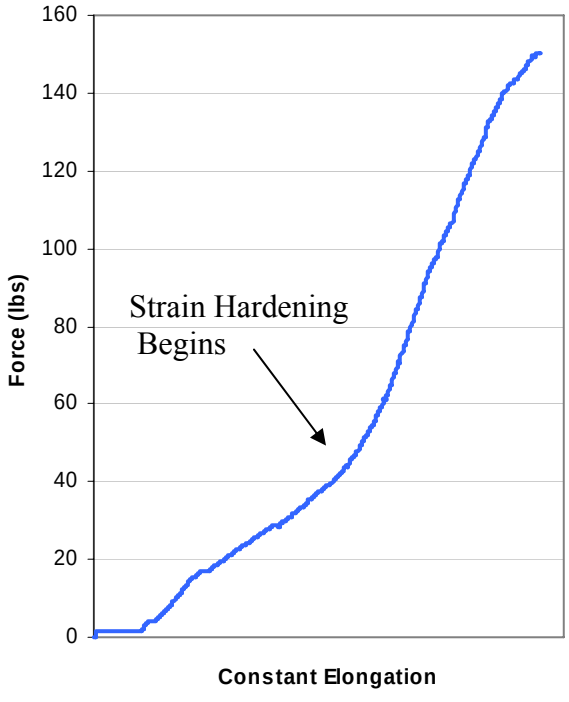

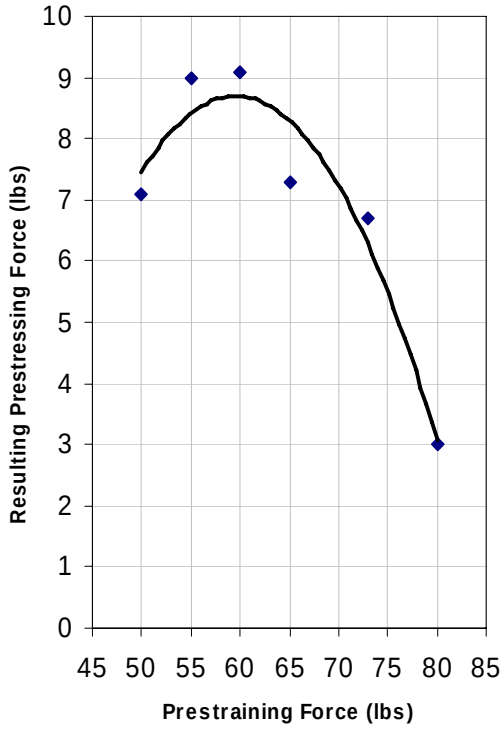

Figure 3.13 – 0.04" SMA Elongation **Figure 3.14 – 0.04" Prestraining Force**

3.3.4.3 Nitinol Prestressing Force

The amount of prestressing in the Nitinol wire was measured at the same time the samples were heated. The wire was connected to the load cell at a fixed length then heated with the heat gun. As the wire warmed up and changed phases, it constricted and a force was applied to the load cell. For the 0.04 inch Nitinol wire, the load peaks when all the material is in the austenite phase. Then, as it cools and returns to martensite, two thirds of the force is lost as seen in Figure 3.15. The 0.04 inch wire retains about 7 pounds per wire prestressing force. The 0.074 inch wire is composed of a different alloy that remains in the austenite phase at room temperature. When it is heated, the 0.74 inch wire peaks at about 77 pounds. When it cools, it only looses around 4 percent of its prestressing force, resulting in 74 pounds of prestressing force per wire.

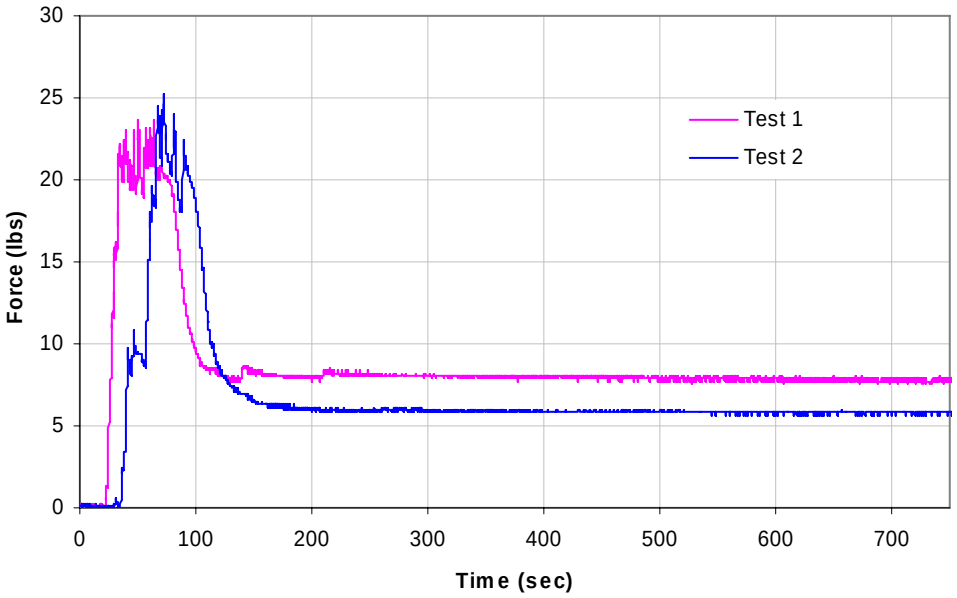

Figure 3.15 – Force in 0.04" SMA Wire During Phase Change

3.4 PRESTRESSING LOSSES

Prestressing Losses, or a decrease in the stress in the prestressing tendon, begin the moment the tendon is stretched. These losses continue for the life of the member, though the rate at which stress is lost decrease with time. For purposes of this experiment, only prestressing losses associated with the pretensioned process will be discussed. Some of these losses occur in the prestressing tendons, while other losses are attributed to the concrete.

3.4.1 Types of Prestressing Losses

The Total Amount of Prestressing Losses (Naaman, 2004):

$$\Delta f_{pT} = \{\Delta f_{pA} + \Delta f_{pR1}\} + \{\Delta f_{pES}\} + \{\Delta f_{pR2} + \Delta f_{pS} + \Delta f_{pC}\} \quad \text{(Eq. 3.9)}$$

$$= \{\text{before transfer}\} + \{\text{during transfer}\} + \{\text{after transfer}\}$$

Where: Δf_{pA} = Stress loss due to anchorage set (tendons)

Δf_{pR1} = Stress loss due to relaxation before transfer (tendons)

Δf_{pES} =Stress loss due to Elastic shortening (concrete)

Δf_{pR2} = Stress loss due to relaxation after transfer (tendons)

Δf_{pS} =Stress loss due to Shrinkage (concrete)

Δf_{pC} = Stress loss due to Creep (concrete)

3.4.1.1 Elastic Shortening

Elastic shortening happens instantaneously. When the forces in the prestressing tendons are transferred to the concrete, stresses develop in the concrete. As the concrete experiences this sudden compression stress, strain develops and the member becomes shorter. Both the concrete and the prestressing tendon experience the same change in strain.

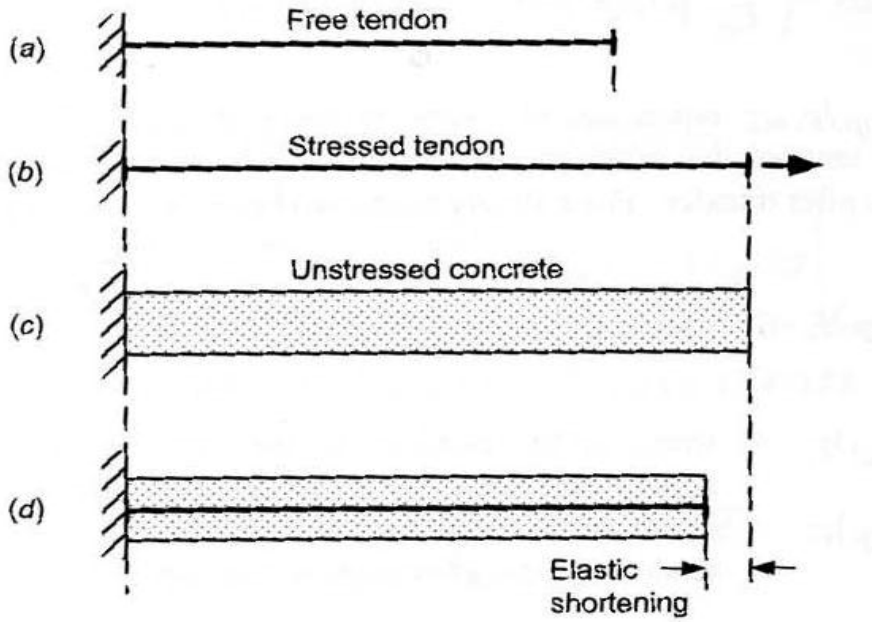

Figure 3.16 – Elastic Shortening Source: Naaman 2004

Prestressing loss due to Elastic Shortening using the Approximate Method (Naaman, 2004):

$$\Delta f_{pES} = \left(\frac{E_{ps}}{E_{ci}}\right)\left(f_{cgp}(F_i + G)\right) \qquad \text{(Eq. 3.10)}$$

Where: E_{ps} = Modulus of Elasticity of Prestressing Strand

E_{ci} = Modulus of Elasticity of Concrete

$(f_{cgp})F_i + G$ = Stress in concrete at the centroid of the prestressing tendon due to the prestressing force and the dead load immediately after transfer.

3.4.1.2 Shrinkage

As a sample cures, excess or free water that is not required for the chemical hydration reaction evaporates. As this water is lost, the sample shortens which reduces the stress in the prestressing tendons. For moist-cured and humidity ranging from 40 to 80%, prestressing losses due to shrinkage over a time interval are found using:

$$\Delta f_{pS}\left(t_i, t_j\right) = E_{ps}\varepsilon_{SU}K_{SH}K_{SS}\left(g(t_j) - g(t_i)\right) \qquad \text{(Eq. 3.11)}$$

Where: E_{ps} = Modulus of Elasticity of Prestressing Strand

ε_{SU} = ultimate shrinkage strain = $2 + \frac{1.1\left(10^{-3}\right)(w - 220)}{230}$

w = water content (lb/yd^3)

K_{SH} = humidity correction factor = 1.4-0.01H

H = humidity (%)

K_{SS} = shape and size factor = $1.14 - 0.09\frac{V}{S} \geq 0.60$

V = volume

S = lateral surface

$g(t) = \frac{t}{35 + t}$

t = time (days)

3.4.1.3 Creep

Creep is the shortening of a sample due to sustained stress. It depends on time, the concrete's properties, and environmental conditions. If the load which caused the sample to creep is removed, part of the creep strain can be recovered with time. Prestressing losses due to creep over a time interval are calculated using:

$$\Delta f_{pC}(t_i, t_j) = \frac{E_{ps}}{E_c} C_{CU} K_{CH} K_{CA} K_{CS} f_{cgp}(t_i)[g(t_i) - g(t_i)] \quad \text{(Eq. 3.12)}$$

Where: E_{ps} = Modulus of Elasticity of Prestressing Strand

E_c= Modulus of Elasticity of Concrete

C_{CU} = ultimate creep coefficient

K_{CH} = humidity correction factor = 1.27-0.0067H

H = humidity (%)

K_{CA} = age at loading factor = $1.25 t_A^{-0.118}$

t_A = age at loading ≥ 7

K_{CS} = shape and size factor $1.14 - 0.09\frac{V}{S} \geq 0.68$

V = volume

S = lateral surface

$f_{cgp}(t_i)$ = stress in the concrete at the center of the prestressing steel at time t_i due to prestressing force and dead load

$g(t) = \frac{t^{0.6}}{10 + t^{0.6}}$

t = time (days)

3.4.1.4 Friction

Friction losses usually occur in post-tensioned members. When the tendon is being stressed, there is a difference in the stress felt by the tendon at each end of the member due to friction between the tendon and the duct. In this experiment, the members are pretensioned, so a duct is not used. However, each tendon wraps around two pulleys. The pulleys are well lubricated and assumed not to produce friction losses when the cable is tensioned.

3.4.1.5 Anchorage Set

Anchorage set is the stress losses produced when "tying off" the prestressing tendon. Typically a wedge-type anchor system is used at the jacking end of a prestressed tendon. When the wedge is locked in, some stress is lost. Another type of anchorage set occurs when multiple strands are used. The strands can not all be tightened simultaneously. The first strand losses some of its prestressing when subsequent tendons are tightened due to elastic shortening or bending of the prestressing bed. In this research, turnbuckles are used to tighten the steel cables. These turnbuckles are attached to calibrated spring scales which read the force in the cable. Because the cable is never "tied off," both types of anchorage set can be avoided. If, after the last turnbuckle is tightened, the first one shows a reduced force, it can be tightened further. Also, the scales are only accurate to two pounds, so a small variation may not even be noticeable.

3.4.1.6 Steel Relaxation

Relaxation is the loss of tension in a tendon of a fixed length. It depends on time, material properties, and environmental conditions. The rate relaxation occurs decreases with time.

$$\Delta f_{pR}\left(t_i, t_j\right) = \frac{f_p t_i}{K}\left(\frac{f_p t_i}{f_{py}} - 0.55\right)\log\left(\frac{t_j}{t_i}\right) \qquad \text{(Eq. 3.13)}$$

Where: $f_p(t)$ = Stress in the prestressing tendon at time t

t = time (hours) and $t \geq 1$

K = constant (10 for stress-relieved and 45 for low-relaxation strands)

f_{py} = Yield strength of prestressing tendon and $\frac{f_p t_i}{f_{py}} \geq 0.55$

3.4.2 Measuring Prestressing Losses

3.4.2.1 Measuring Elastic Shortening, Shrinkage, and Creep

Elastic shortening, shrinkage, and creep were directly measured from the samples. Special nylon or brass screws were cast into the beams. Two beams were cast of each sample type. One beam of the beams had screws on all four sides and the other beam only had screws on the top and bottom. Two control beams were also cast with the same screw configuration. The distance between the screws was measured four times: before and after applying the prestressing forces, after 7 days, and again after 14 days. The dial gauges used to measure the change in distance between the screws is accurate to the 0.0001 of an inch and is shown in Figure 3.17.

Figure 3.17 – Dial Gauge

3.4.2.2 Measuring Steel Relaxation

The steel relaxation was measured experimentally. Two cables of each size where stretched in the prestressing bed. Each wire had 200 pounds of force initially. Because the wires were attached to a spring scale, the length would change as the cable relaxed. To keep the length from changing, the force was reduced as the cable relaxed. The relaxation was measured for 2 weeks. This produced a rough estimate of the amount of relaxation that occurs in the cables and also confirmed that the majority of the relaxation occurs during the first day as seen in Figure 3.18. For a more accurate amount of relaxation, cables were tested using the load cell and a fixed distance.

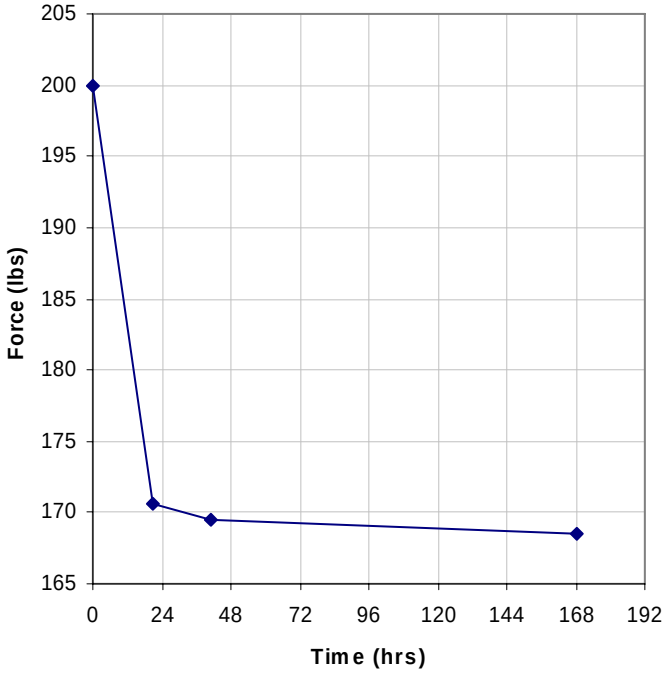

Figure 3.18 – 3/64" Steel Cable Relaxation

3.5 PRESTRESSING BED

The prestressing bed seen in Figures 3.19 and 3.20 makes up to 6 beams at a time. The beams are 4 inches wide, 1 inch tall, and 24 inches long. Each cable was secured around piano pegs at end A. The cables then go through 2 metal and 4 plastic spacers as seen in Figure 3.20 at location B. The cables wrap around a pulley at end C and feed pack through the spacers. At end A they make a 90 degree bend around another pulley and attach to a turnbuckle and a spring scale. The turnbuckle is then tightened to stress the cable and the force can be read on the spring scale.

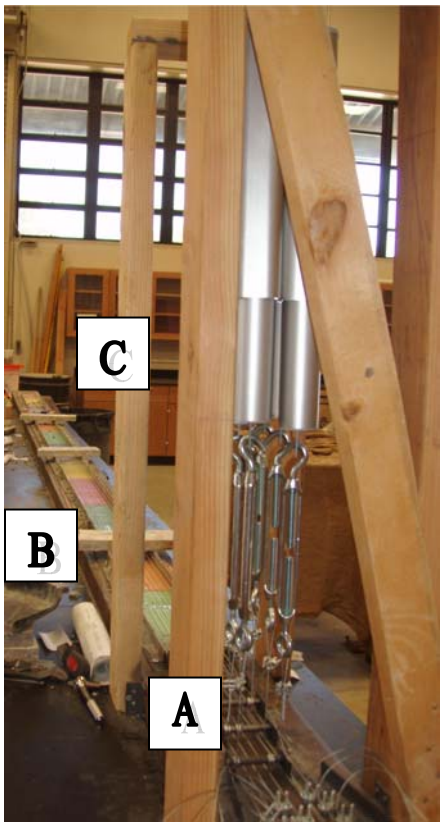

Figure 3.19 – Prestressing Bed

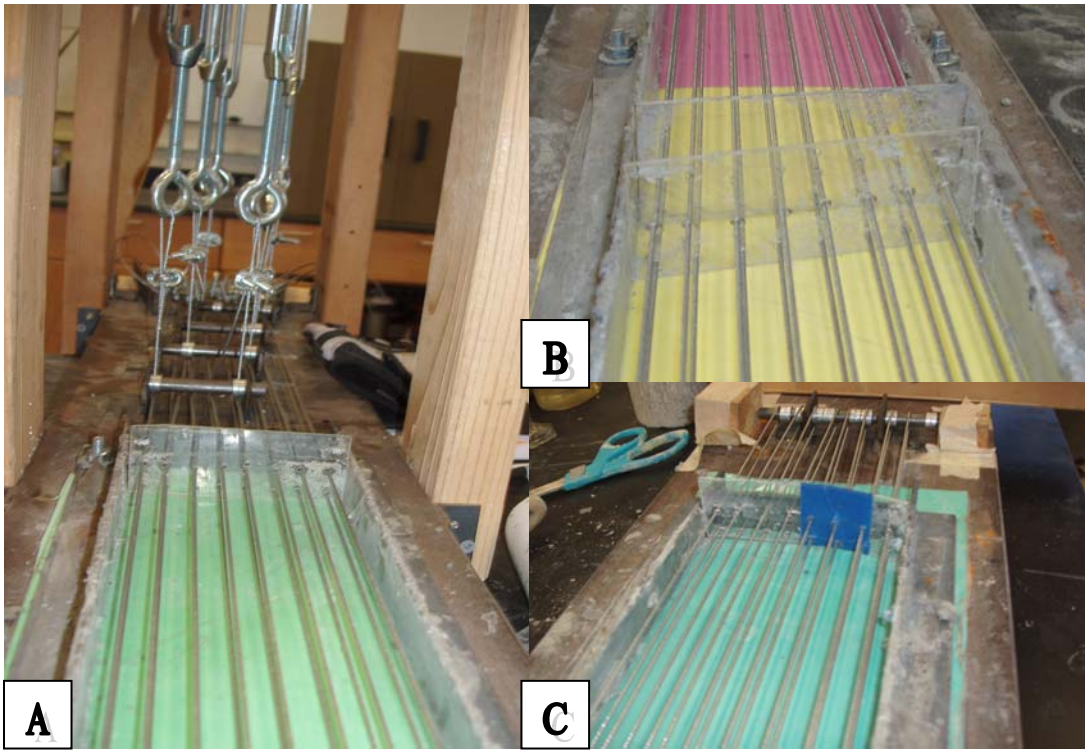

Figure 3.20 – Prestressing Bed Detail

Prior to breaking samples, they are measured with an electric scale which is accurate to .0001 of an inch as shown in Figure 3.21. The shrinkage, creep, and elastic shortening are measured with the dial gage as discussed in section 3.3.2.1 through 3.3.2.3. The dynamic modulus of elasticity is measured as described in section 3.2.1.3, and the sample is weighed. Two concrete cylinders are tested to determine the ultimate compressive strength of the concrete.

Figure 3.21 – Electric Scale

A third-point bending test is used to test the samples. The base roller supports are 18 inches apart and there is a 3 inch overhang at each end on the beam. The top 2 rollers are separated by 6 inches, which divides the middle of the beam into 3 equal sections. A steel plate spans the top rollers and a 2000 pound load cell is attached to the test machine and is accurate to the 0.1 of a pound. Deflection is measured with 4 linear variable differential transformers (LVDT's) which measure to the 10^{-7} of an inch. A LVDT is located at each end above the base roller supports, and two LVDT's are located at the

center of the beam. Figure 3.22 shows the test set-up. The beams from the first portion of the testing, which were prestressed with steel cables, were loaded at 2 pounds per second until failure. The beams prestressed with SMA wire or fibers were loaded under displacement control at a rate of .002 inches per second. The samples with straight Nitinol wires were loaded until the deflection reached 0.36 inches which is about 65 percent of the ultimate deflection the sample can withstand before failure. Similarly, the Nitinol fiber prestressed samples were loaded until deflection reached 0.2 inches or around 36 percent of the ultimate deflection. All of the SMA prestressed samples were reheated using a heat gun after the initial loading. Any recovery the samples made was recorded. The samples were then tested a second time. Following this, the samples were reheated in the oven, crack closure was examined, and the samples were loaded one final time.

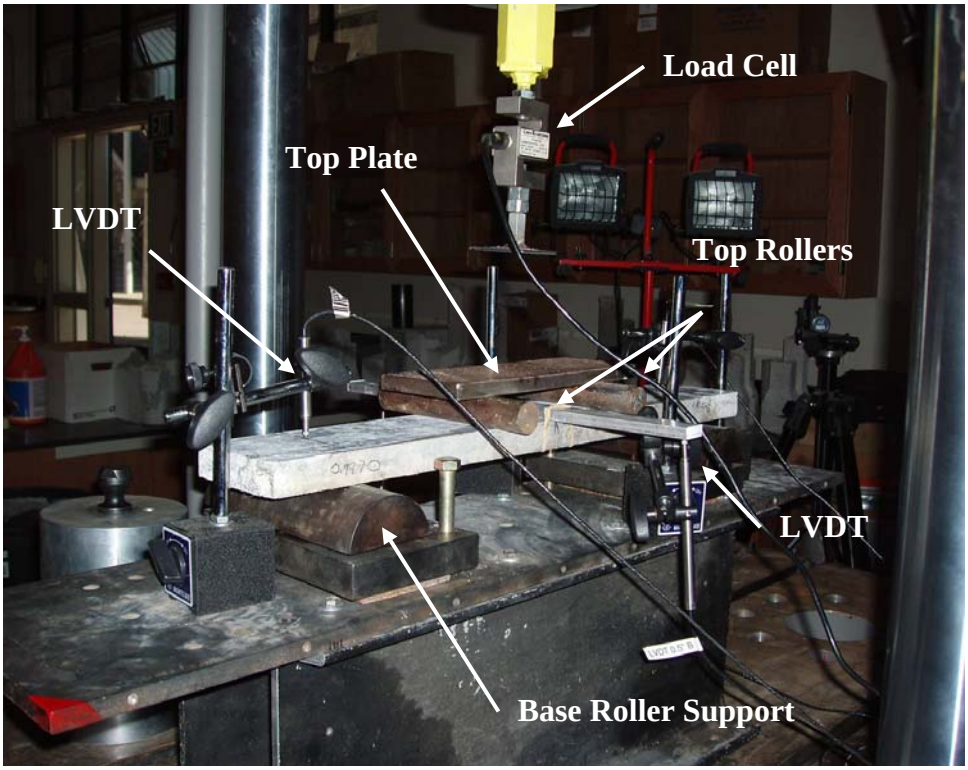

Figure 3.22 – Third Point Bending Test

Chapter 4
Analysis and Results

4.1 INTRODUCTION

The experiments are separated into two parts. In the first portion, concrete was prestressed using steel cables. Two different sized cables were used: 1/16 (0.0625) inch diameter and 3/64 (0.0469) inch diameter. The prestressing load applied to the cables along with the cable size was varied in each test. As seen in Table 4.1, the first six tests were released after two days. The seventh batch was left in the prestressing bed for two weeks before the cables were released and the prestressing force was applied to the concrete. For the second portion of testing, Shape Memory Alloy (SMA) wires were used to prestress the concrete. It was tested both as straight, continuous wires and as discrete random fibers. Two different SMA wires were used. The first SMA wire has a 0.04 inch diameter and was composed of Nitinol alloy M, which is in the martensite phase at room temperature. A 0.75 inch diameter SMA wire was also used which as composed of Nitinol alloy X, which can be either martensite or austenite at room temperature. Steel fibers (non-prestressed) were also used. Tests were run using only SMA fibers, only steel

fibers, and combinations of the two types. Table 4.1 shows a summary of the tests performed in both portions of the experiment and Figure 4.1 shows the location of the wires in each test case.

Table 4.1 – Summary of Tests

	Specimen	Wire Size	Prestressing Load per Wire (lbs)*	Number of Cables	Percent Reinforcement by Volume (%)	Total Initial Load (lbs)	Test Days [Release] (days)†
PART 1	1/16-0	1/16 Steel Cable	0	16	0.41	0	[2], 7, 14
	1/16-10	1/16 Steel Cable	10	16	0.41	160	[2], 7, 14
	1/16-200	1/16 Steel Cable	200	16	0.41	3200	[2], 7, 14
	1/16-240	1/16 Steel Cable	240	16	0.41	3840	[2], 7, 14
	3/64-150	3/64 Steel Cable	150	16	0.26	2400	[2], 7, 14
	3/64-200	3/64 Steel Cable	200	16	0.26	3200	[2], 7, 14
	3/64-200B	3/64 Steel Cable	200	16	0.26	3200	[14], 28
PART 2	SF1	Steel Fibers	0	Fibers	1.77	0	2, 7, 14
	SF2	Steel Fibers	0	Fibers	2.41	0	2, 7, 14
	0.04-ST	0.04 SMA	7	67	2.01	470	[14]
	0.04-F1	0.04 SMA	7	Fibers	1.57	330	[14]
	0.04-F2	0.04 SMA + Steel Fibers	7	Fibers	0.47 SMA + 1.09 Steel	120	[14]
	0.075-St	0.075 SMA	74	10	1.19	740	[14]
	0.075-F1	0.075 SMA	74	Fibers	1.47	---	[14]
	0.075-F2	0.075 SMA	74	Fibers	1.92	---	[14]

* The prestressing load in the cables is the force read from the spring scale in section 3.4 and the load in the SMA wires is from the phase change described in Section 3.2.4.2. This value does not include prestressing losses.

† Two samples were broken on each test day.

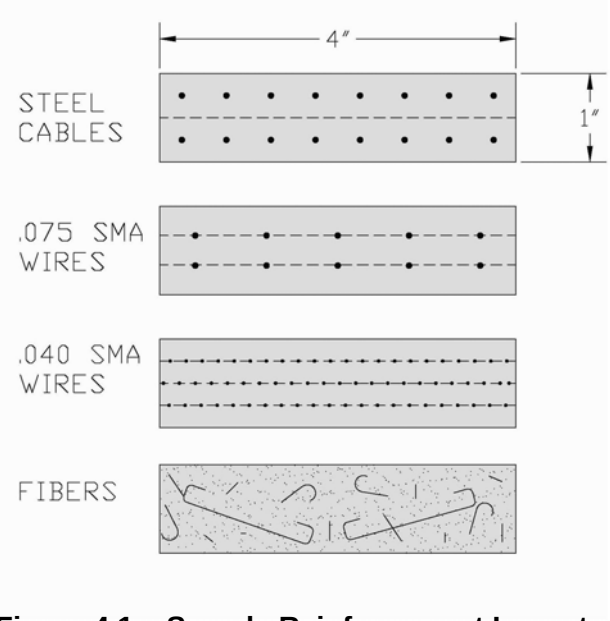

Figure 4.1 – Sample Reinforcement Layout

4.2 ELASTIC SHORTENING AND CONCRETE SHRINKAGE

The amount of elastic shortening in each sample is related to the amount of prestressing in the sample along with the modulus of elasticity of the concrete (E_c) and the steel or Nitinol (E_s). As expected, the samples with no prestressing, MOR and 1/16_0, had the lowest amount of shortening as seen in Table 4.2 and Figure 4.2. Increasing E_c decreases the amount of elastic shortening that occurs in a sample. This can be seen in samples 3/64_200 and 3/64_200B. The release day was varied between these two samples so E_c of 3/64_200B was higher at release which reduced the amount to elastic shortening. As seen in samples 1/16_200 and 3/64_200, when E_s increases, so does the amount of elastic shortening in a sample. The Nitinol samples have a high E_c and low E_s, but they have the added shrinkage from baking in the oven.

Table 4.2 – Elastic Shortening and Concrete Shrinkage at Release

Sample	Elastic Shortening and Shrinkage (in)
MOR	0.00045
1/16_0	0.00055
1/16_10	0.00095
1/16_200	0.00280
1/16_240	0.00205
3/64_150	0.00575
3/64_200	0.00595
3/64_200B	0.00160
.04 SMA Straight	0.00218
.04 SMA Fiber	0.00213
.04 SMA & Steel Fiber	0.00135
.075 SMA Straight	0.00150
.075 SMA 2% Fiber	0.00133
.075 SMA 1.5% Fiber	0.00180

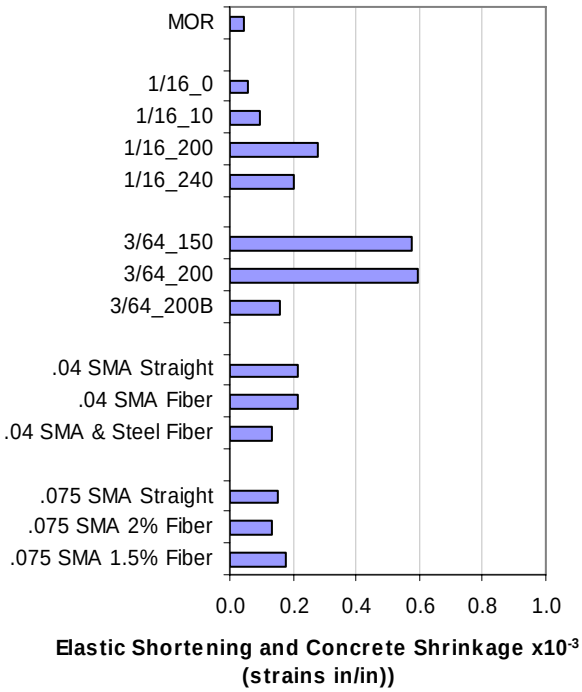

Figure 4.2 – Elastic Shortening and Concrete Shrinkage at Release

Figure 4.3 compares the measured elastic shortening and concrete shrinkage to the theoretical elastic shortening. The SMA samples experienced more shrinkage because they were thermally treated in the oven.

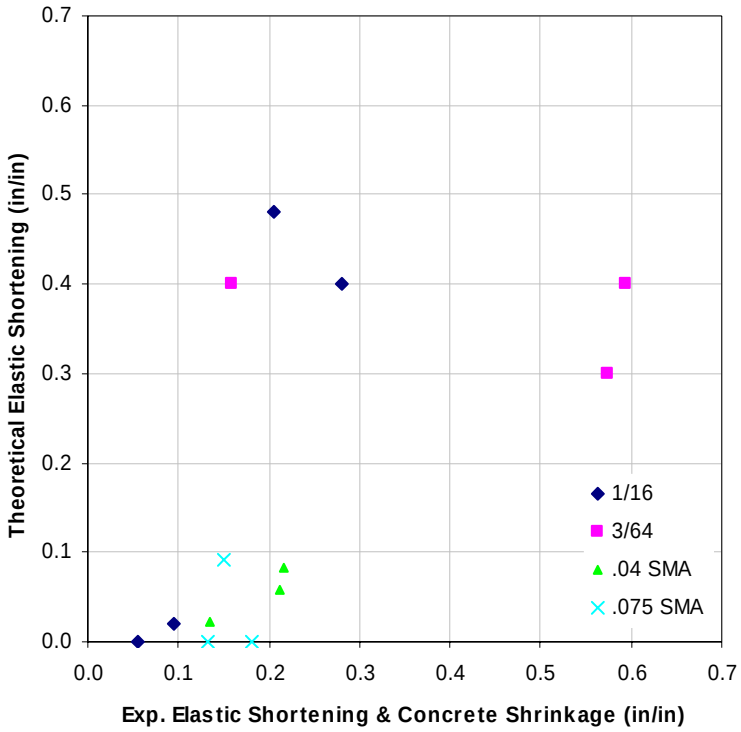

Figure 4.3 – Experimental Elastic Shortening and Shrinkage versus Theoretical Elastic Shortening

4.3 INITIAL CRACK

4.3.1 Determining Experimental Bending Stress at Initial Crack

The force at initial crack was determined using the graphs from the third point bending tests. As seen below in Figure 4.4, the line has a very steep slope initially. When the member cracks, the slope changes quite drastically. The initial crack for the 7 day test using 1/16 inch cable and 200 pounds initial prestressing occurs around 305 pounds, as seen below. The bending stress is then determined using Equation 3.8.

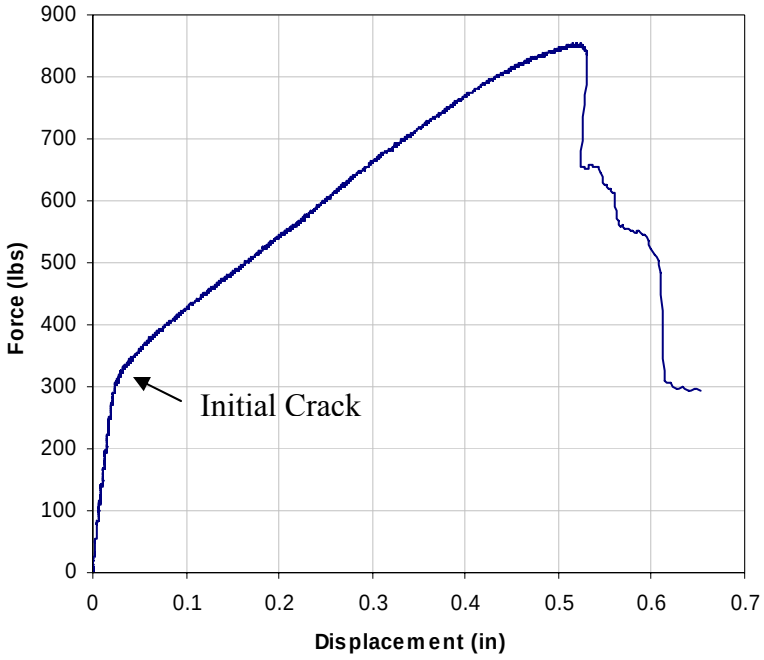

Figure 4.4 – Initial Cracking Force of 7 Day Prestressed Sample During Third Point Bending Test

As seen in Figure 4.5, slope of the force-displacement curve does not change with prestressing, but as the amount of prestressing increases, the force required to crack the sample increases. The displacement of the sample is reduced when prestressing is added to the sample, while the ultimate load at failure remains unaffected. Table 4.3 contains the force required to crack each sample along with the compressive strength of the concrete when the sample was tested.

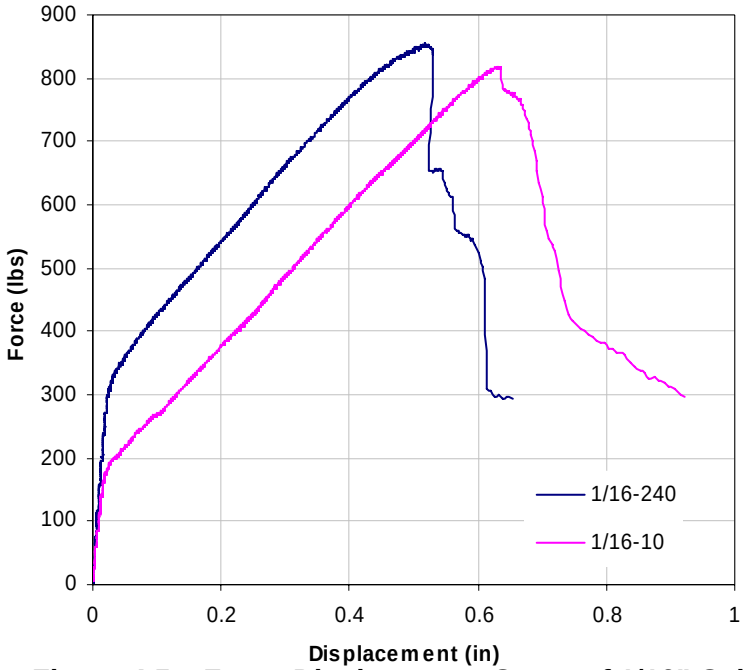

Figure 4.5 – Force-Displacement Curve of 1/16" Cable with Varied Prestressing Force

Table 4.3 –Initial Cracking Force

Specimen	2 day			7 day			14 day		
	Test 1 (lbs)	Test 2 (lbs)	Comp. Strength (psi)	Test 3 (lbs)	Test 4 (lbs)	Comp. Strength (psi)	Test 5 (lbs)	Test 6 (lbs)	Comp. Strength (psi)
1/16-10	110	84	3205	213	134	6418	205	179	7031
1/16-200	266	249	3798	305	307	5621	334	356	6588
1/16-240	289	241	3824	222	316	6119	301	269	7005
3/64-150	215	147	2850	194	267	5125	221	265	5213
3/64-200	256	184	2998	258	240	4597	284	281	5419
3/64-200B							311	319	6036
0.04-ST							199	156	4342
0.075-ST							197	103	6545

The bending stress in the Nitinol was determined the same way as the steel cables. When compared to the samples reinforced with steel cables, the slope of the force-displacement curve of the Nitinol samples is not as steep, as illustrated in Figure 4.6. The sample prestressed with the Nitinol cracks at a higher force then the 1/16-10 sample which essentially has no prestressing. The sudden drops in the Nitinol curve just after cracking indicate that the wire may be slipping inside the sample. The Nitinol samples were not tested to failure so the unloading curve is seen in Figure 4.6. At the same amount of displacement, the forces in the steel cable samples are roughly double the force in the Nitinol samples.

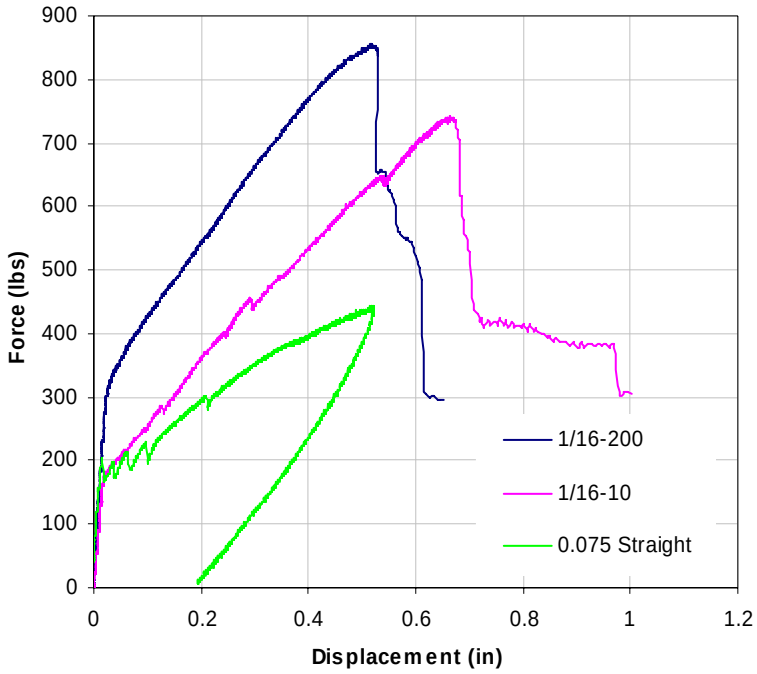

Figure 4.6 – Force-Displacement Curve of 1/16" Cable versus Nitinol Wire

4.3.1.1 Initial Crack – Varying Prestressing Force

As the initial prestressing force increased, the stress when the first cracks formed also increased. Figures 4.7 and 4.8 below, graph the compressive strength of the concrete versus the first crack stress. Each point corresponds to a different age at testing (ex. 2 day, 7 day, etc.). As seen in the graphs, all the lines have the same slope, which corresponds to the change in the modulus of rupture. This is expected because the only difference in the samples is the amount of prestressing. The concrete mix used for all of the samples is the same.

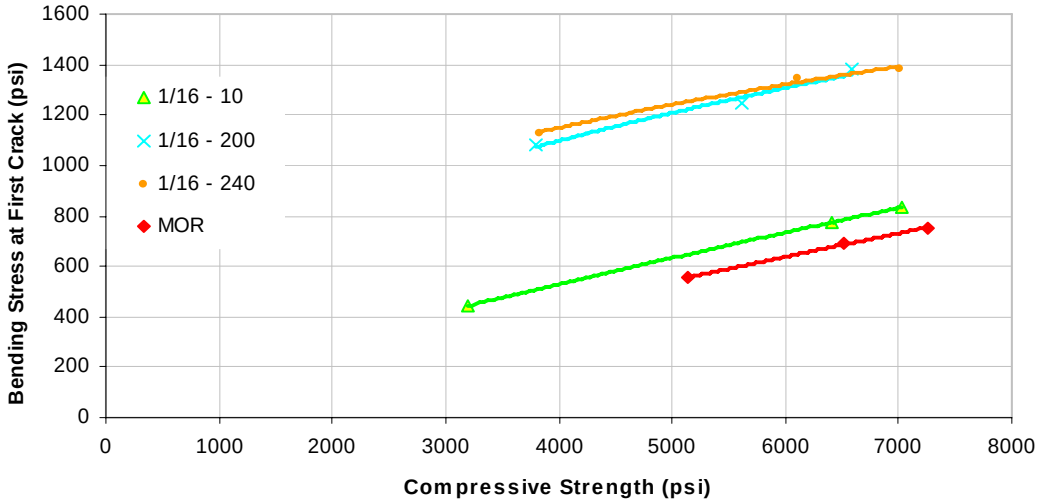

Figure 4.7 – 1/16" Cable with Varied Prestressing Force

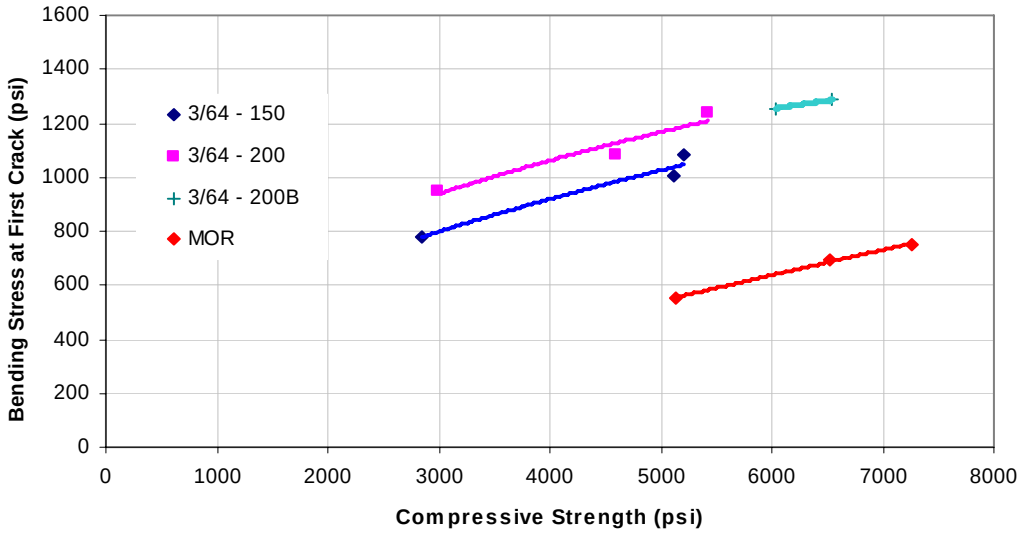

Figure 4.8 – 3/64" Cable with Varied Prestressing Force

4.3.1.2 Initial Crack – Varying Release Date

Varying the release date has little effect on the bending stress at first crack. How much stress the member can take before cracking is influenced by the compressive strength of the concrete and the amount of prestressing applied to the member. In Figure 4.9, both sets of samples have the same amount of initial prestressing, but one set was released after 2 days in the prestressing bed, while the second set was released after 14 days. The compressive strength of the concrete at release was 3700 and 6750 for the 2 day and 14 day test, respectively. The 14 day release line is almost a continuation of the 2 day release line. The main difference between the two release dates is the amount of elastic shortening that occurs. As expect, due to the increased compressive strength of the concrete, the 14 day release samples experienced substantially less elastic shortening then the 2 day release samples. When samples were demolded and the prestressing forces were transferred to the concrete, the 2 day release samples shrank 0.00595 inches, which is four times more then the 14 day samples which shrank 0.0016 inches. This value includes the elastic shortening along with some shrinkage in the concrete.

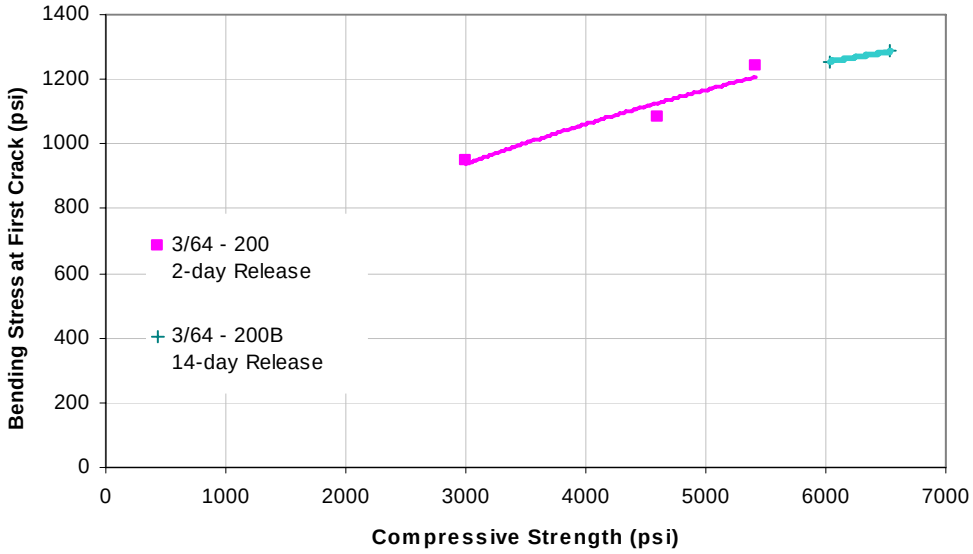

Figure 4.9 – 3/64" Cable with Varied Release Time

4.3.1.3 Initial Crack – Varying Cable Size

The size of the cable has little effect on the initial crack on the concrete. For the same initial prestressing force, the two cables resulted in very similar first crack stresses (see Figure 4.10). This is expected because the wire properties like modulus of elasticity and ultimate strength do not affect the sample until after the concrete has cracked. While the steel relaxation varied slightly between the two cables, the 1/16 inch cable relaxed 2.5 percent more then the 3/64 inch cable, this does not seem to have much effect on the prestressing force.

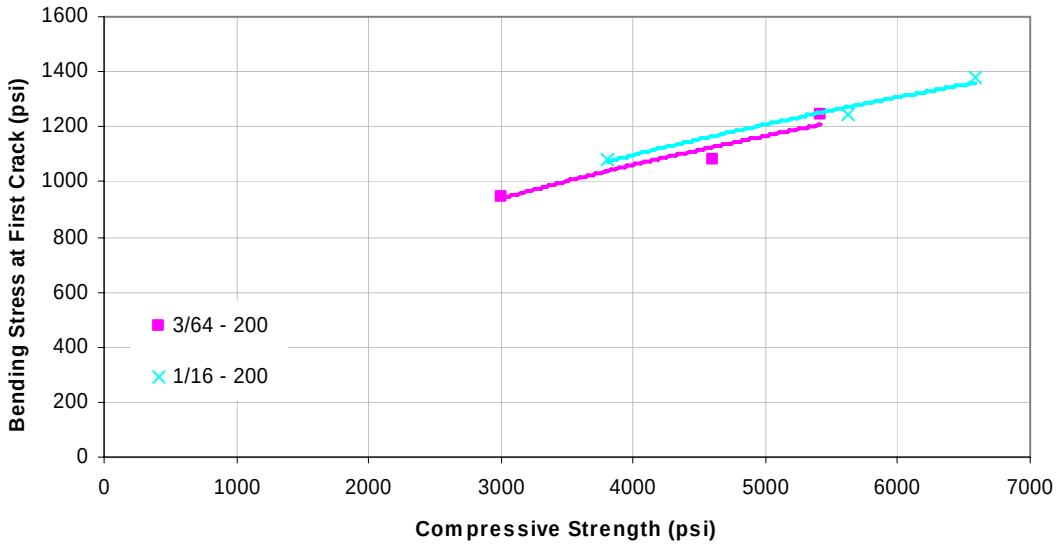

Figure 4.10 – Varied Cable Size with the Same Prestressing Force

4.3.1.4 Initial Crack – Steel Cable versus Nitinol Wire

The Nitinol wire applies a prestressing force to the concrete. Figure 4.11 shows the 0.04 inch and 0.075 inch Nitinol wire as points above the modulus of rupture (MOR) line. The distance the points are offset from the MOR line indicates the amount of prestressing in the sample. As seen in Table 4.1, the 3/64 inch steel cable samples had a four times higher prestressing force then the Nitinol samples which is also evident in the figure. The amount of prestressing in the Nitinol samples is based on the amount of wire in the sample. The 0.04 inch Nitinol sample with straight wires running the length of the sample was two percent Nitinol by volume which is eight times more prestressing material then the steel cable which were 0.25 percent of the sample by volume. To get the same amount of prestressing from the Nitinol alloys used in these samples, 30 times more prestressing material must be used.

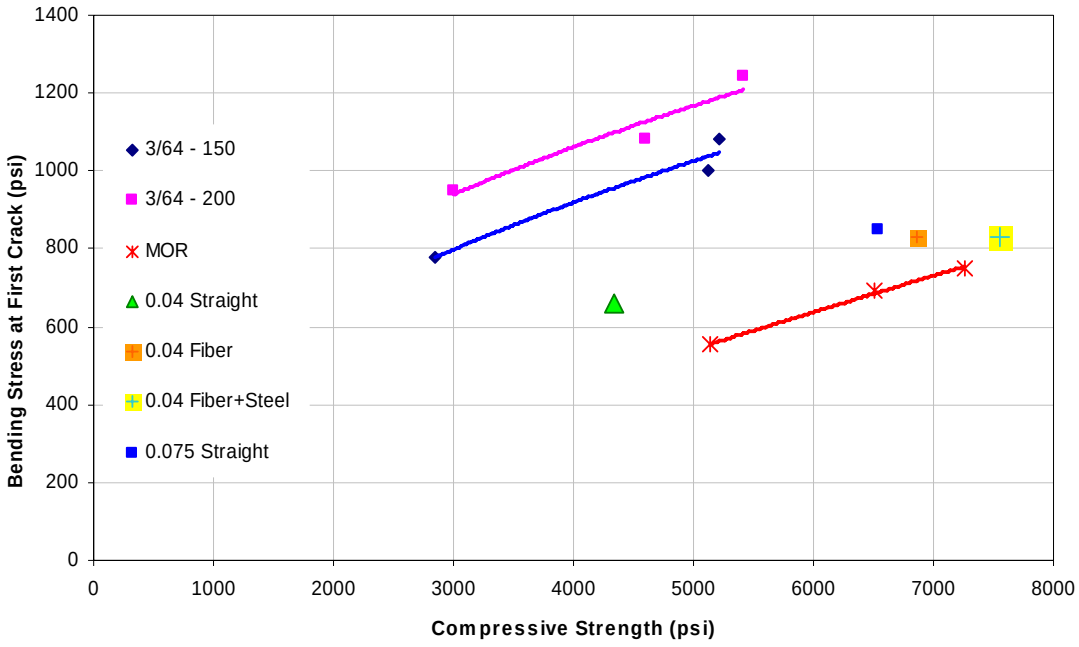

Figure 4.11 – Prestressing with Steel Cables versus SMA Wires and Fibers

4.3.1.5 Initial Crack – Theoretical versus Experimental

The experimental initial crack values are very similar to those expected using Equation 3.7a. The prestressing force was determined using the initial prestressing force in the cables or wires minus the measured prestressing losses. As seen in Table 4.4, the average percent error for the steel cable samples is relatively low. Negative values indicate that the sample cracked at a higher load then the predicted load. Similarly, a positive percent error indicates the sample cracked at a lower load. As expected, there is a fairly even distribution of positive and negative percent error values. The Nitinol samples at the bottom of Table 4.4 show a larger average percent error. In each case, one of the samples cracked within four percent of the expected value. Because of the limit number of Nitinol samples, it is hard to tell if these are just outliers or if there is a lot of variation in the Nitinol samples.

Table 4.4 – Initial Crack Percent Error

Specimen	2 day		7 day		14 day		Average Error
	1	2	3	4	5	6	
1/16-10	-25	6	-31	15	-15	-1	-9
1/16-200	-8	-1	-4	-2	-2	-11	-5
1/16-240	-9	8	30	0.3	9	9	8
3/64-150	-15	18	15	-11	6	-16	-0.3
3/64-200	-13	18	2	8	1	-5	2
3/64-200B					-1	-1	-1
0.04-ST					-28	-4	-16
0.075-ST					2	51	26

4.3.1.6 Initial Crack – Prestressing Force

The amount of prestressing in each sample was calculated using Equation 3.7b. The experimental initial crack values of the two day test samples were used to solve for the prestressing force in the sample. Table 4.5 shows the theoretical prestressing force applied to each sample based on the scales for the cables and testing for the Nitinol. The experimental prestressing force was then calculated and compared to the expected amount of prestressing in the sample. All of the steel cable samples had low percent errors, so there was little difference between the applied prestressing force and the force back-calculated from the bending stress at initial crack. The Nitinol samples, one the other hand, displayed a large variation. Seven of the twelve Nitinol sample showed no prestressing. The 0.075 inch Nitinol fiber samples cracked around the fibers. The hooks, also add stress to the samples because they were trying to straighten, which may have resulted in their contributed to the early failure. Both of the 0.04 inch Nitinol samples with continuous straight wires prestressing the sample resulted in a higher prestressing

Table 4.5– Applied versus Experimental Prestressing Force

Specimen	Theoretical Prestressing Force (lbs)	Sample 1			Sample 2		
		Experimental Prestressing Force (lbs)	Difference (lbs)	Percent Error	Experimental Prestressing Force (lbs)	Difference (lbs)	Percent Error
1/16-10	160	650	-490	-306%	175	-15	-9%
1/16-200	3200	3325	-125	-4%	3800	-600	-19%
1/16-240	3840	3350	490	13%	3350	490	13%
3/64-150	2400	2125	275	11%	3050	-650	-27%
3/64-200	3160	3100	60	2%	3400	-240	-8%
3/64-200B	3140	3180	-40	-1%	3180	-40	-1%
.04 Straight	670	1425	-755	-113%	775	-105	-16%
.075 Straight	741	680	61	8%	0	741	100%
.04 Fiber 1	---	470		---	0		---
.04 Fiber 2	---	0		---	180		---
.075 Fiber 1 & 2	---	0		---	0		---

force than expected. Pull-out test determine that the 0.04 inch Nitinol fibers were not slipping inside the sample, so either the samples are cracking around the fibers, the concrete is weakened from thermally processing it in the oven, there is added stress due to the hooks trying to straighten, or a combination of these problems. The prestressing with nitinol increases the initial crack by 30 percent, but the concrete is weakened by 11 percent when it is heated in the oven.

4.4 LOAD-DEFLECTION RESPONSE

4.4.1 Theoretical Model of Moment-Curvature Curve

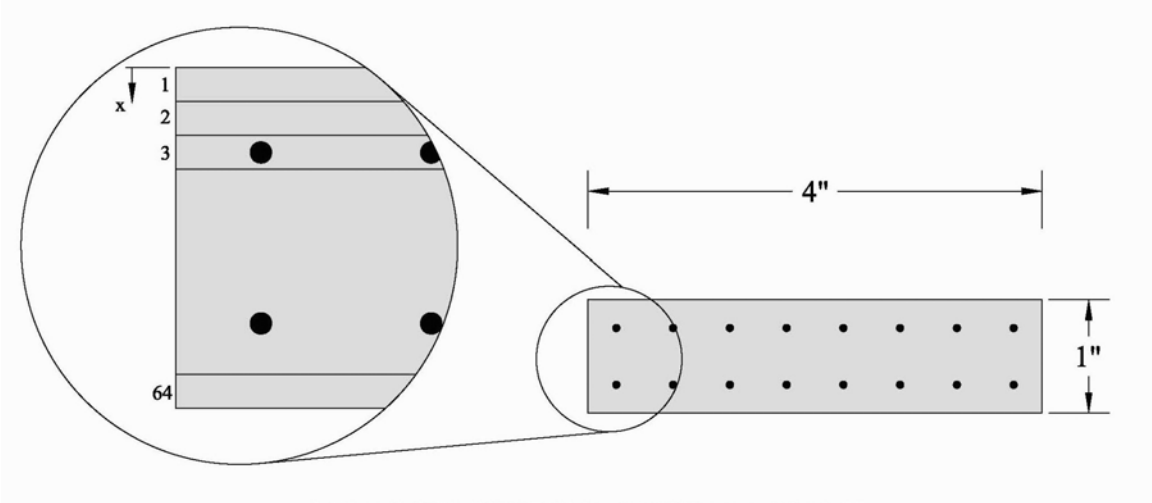

Figure 4.12 – Sample Divided into 64 Layers for Theoretical Analysis

The steel cable samples were also modeled using sections. The sample was divided into 64 layers ass seen in Figure 4.12. The strain at the top of the member was varied from 0.0003 to 0.0047 or member failure. Carreira and Chu's stress-strain relationship (1985) was used to model the stress in the concrete:

When: $\varepsilon_c < MOR$ $\sigma_c = 0$ (Eq. 4.1)

$MOR < \varepsilon_c < 0$ $\sigma_c = \varepsilon_c E_C$ (Eq. 4.2)

$0 < \varepsilon_c < fc'$ $$\sigma_c = f_c' \frac{\beta \frac{\varepsilon_c}{\varepsilon_c'}}{\beta - \left(\frac{\varepsilon_c}{\varepsilon_c'}\right)^{\beta}}$$ (Eq. 4.3)

$f_c' < \varepsilon_c$ $\sigma_c = 0$ (Eq. 4.4)

Where: ε_c = Strain of Concrete in in/in

MOR = Modulus of Rupture in psi

σ_c = Stress in Concrete in psi

f_c' = Compressive Strength of Concrete in psi

$$\beta = \frac{1}{1 - \frac{f_c'}{\varepsilon_c' E_c}}$$

$$\varepsilon_c' = 0.002 + 0.001\frac{f_c' - 4000}{8000}$$

E_C = Static Modulus of Elasticity of Concrete

Carreira and Chu's stress-strain relationship was chosen for a number of reasons. As seen in Figure 4.13, equation 4.3 is a continuous equation because it describes the stress-strain relationship on both sides of the peak. One of the main differences in concrete stress-strain models is the behavior of the curve post-peak. The samples model in this research had maximum strains from 0.0018 in/in to 0.0045 in/in. Most of these maximum strains fall on the post-peak section of the graph. Because the results using Carreira and Chu's model fit the experiment data very well, the post peak curve is very similar to the actual stress-strain curve of the concrete. Trying to find a more accurate model would have little effect on the final results.

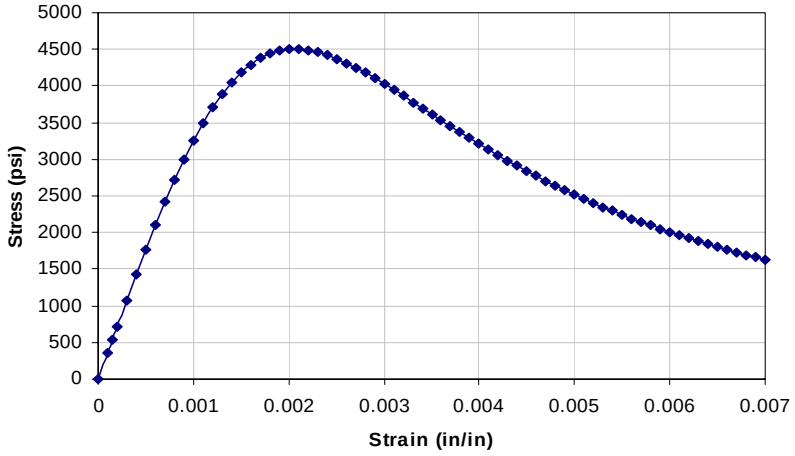

Figure 4.13 – Carreira and Chu's Stress-Strain Relationship

For each strain, the force at each of the 64 sections was calculated using the material properties of the concrete and steel cables.

$$dF_{ci} = A_{ci}\sigma_c \quad \text{(Eq. 4.5)}$$

$$dF_{si} = A_{si}\sigma_s \quad \text{(Eq. 4.6)}$$

Where: dF_{ci} = Force in the Concrete at Section i in pounds

A_{ci} = Area of Concrete in Section i in in^2

dF_{si} = Force in the Steel at Section i in pounds

A_{si} = Area of Steel in Section i in in^2

$\sigma_c = \varepsilon_s * E_S - \frac{F_s}{A_s}$ = Stress in Steel in psi

ε_s = Strain in the Steel in in/in

E_S = Modulus of Elasticity of Steel Cable in psi

Fs = Prestressing Force in pounds

As = Total Area of Steel in in^2

Excel was then used to set the sum of the forces to zero by moving the neutral axis up or down in the sample. The moment is then calculated as the sum of the force in each section times the area of the section and the distance the force is from the top edge of the sample.

$$M = \sum_{i=1}^{n}\left(dF_{ci}\,y_i + dF_{si}\,y_i\right) \quad \text{(Eq. 4.7)}$$

Where: y_i = Distance from the top of the sample to the center of the layer in inches

The moment was then compared to the curvature (strain/distance to the neutral axis) as seen in Figure 4.14. The sudden change in slopes is the theoretical moment when the sample cracks. The moment was then multiplied by 6 and divided by the length between supports to calculate the load on the member. The load when the sample cracked along with the maximum load the sample felt were compared to the experimental force at initial crack and the force at failure respectively as seen in Table 4.6. This model is fairly accurate for the load when the sample cracks. Because these samples are thin and fail under relatively low loads, the higher percent errors for the failure force were expected. The failure modes were also compared; either the concrete crushed in compression or the steel yielded and broke in tension. In all cases, the predicted failure mode matched that seen in the experiments.

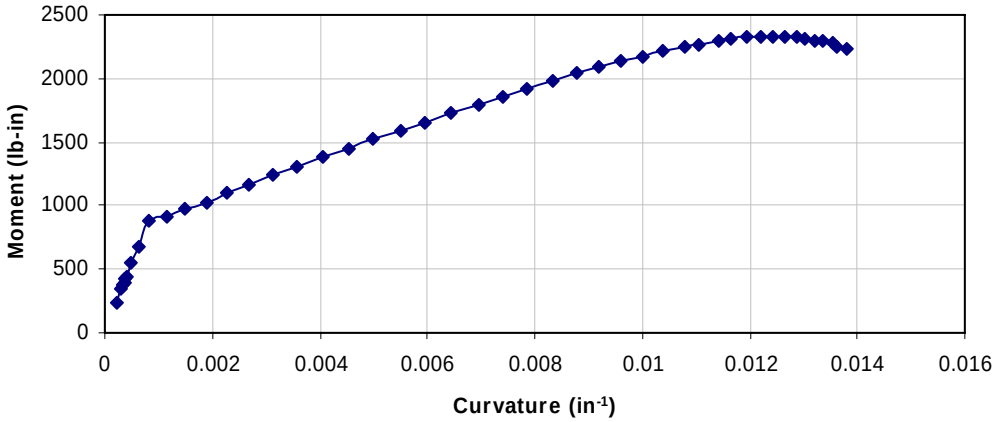

Figure 4.14 – Theoretical Moment-Curvature Curve for 7 day 1/16-240

Table 4.6 – Percent Error and Failure Mode

Specimen	Ave. Crack Error	Ave. Failure Error	Failure Mode		
			2 day	7 day	14 day
1_16-10	2%	7%	Compression	Compression	Compression
1_16-200	6%	14%	Compression	Compression	Compression
1_16-240	-7%	-27%	Compression	Compression	Compression
3_64-150	-7%	8%	Compression	Compression	Tension
3_64-200	-7%	20%	Tension	Tension	Tension

4.4.2 Theoretical Model of Force-Displacement Curve

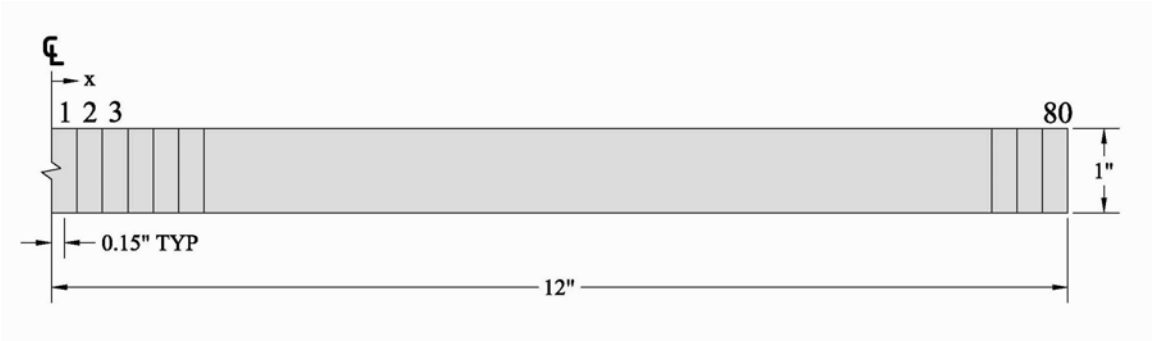

Figure 4.15 – Sample Divided into 0.15" Sections Lengthwise

The sample's deflection was then predicted using the moment-curvature data. The sample was divided into 0.15 inch sections lengthwise as shown in Figure 4.15. The moment was then calculated based on a load applied during third-point bending. The load varied in five pound increments from zero to the predicted failure.

$$M = \frac{PL}{6} \qquad \text{when} \frac{L}{3} < x < \frac{2L}{3} \qquad \text{(Eq. 4.8)}$$

$$M = \frac{Px}{2} \qquad \text{when } x < \frac{L}{3} \qquad \text{(Eq. 4.9)}$$

$$M = \frac{P(L-x)}{2} \qquad \text{when } \frac{2L}{3} < x \qquad \text{(Eq. 4.10)}$$

Where: M = moment in psi

P = load in pounds

L = length between supports = 18 inches

x = distance from support in inches

The curvature was then linearly interpolated from the moment-curvature data calculated previously. The slope at the midpoint on each sliver was then calculated:

$$S_1 = \frac{C_1 \Delta x}{2} \qquad \text{(Eq. 4.11)}$$

$$S_n = S_1 + \sum_{i=2}^{n} \frac{(C_i + C_{i-1})\Delta x}{2} \qquad \text{(Eq. 4.12)}$$

Where: S = slope in radians

C = curvature of the section in in/in

Δx = length of the segment = 0.15 inches

The deflection was then calculated:

$$D = \Delta x \sum_{i=1}^{60} S_i \qquad \text{(Eq. 4.13)}$$

Figure 4.16 compares the predicted load versus deflection curves to the experimental curve. This sample has essentially no prestressing. The predicted model has a sudden change in slope at about 100 pounds. This is the estimated load at initial crack occurs. The predicted value is lower then the experimental and the sharp change in slope is because the model assumes that the concrete takes no tension once it reaches the modulus of rupture. Realistically, the concrete still takes some tension after it cracks.

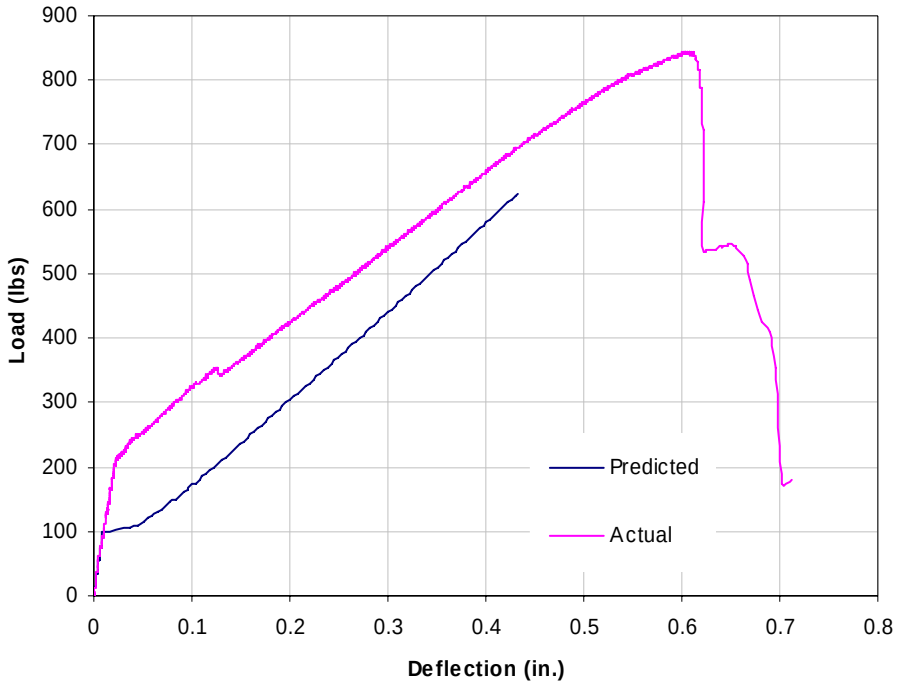

Figure 4.16 – Load-deflection curve for 1/16-10 14 day

The prestressed samples followed the predicted curve very well. The slopes of the curves in Figures 4.17 and 4.18 are very similar along with the load required to crack the samples. This model is only accurate for the first portion of the load-deflection curve. It is not designed to predict the load-deflection at failure. Both of these figures confirm that the theoretical model is fairly accurate. Figure 4.17 has a sharp transition between slopes when the sample cracks while Figure 4.18 has a more gradual change. In both cases, the predicted curve was able to match this change in slope very accurately.

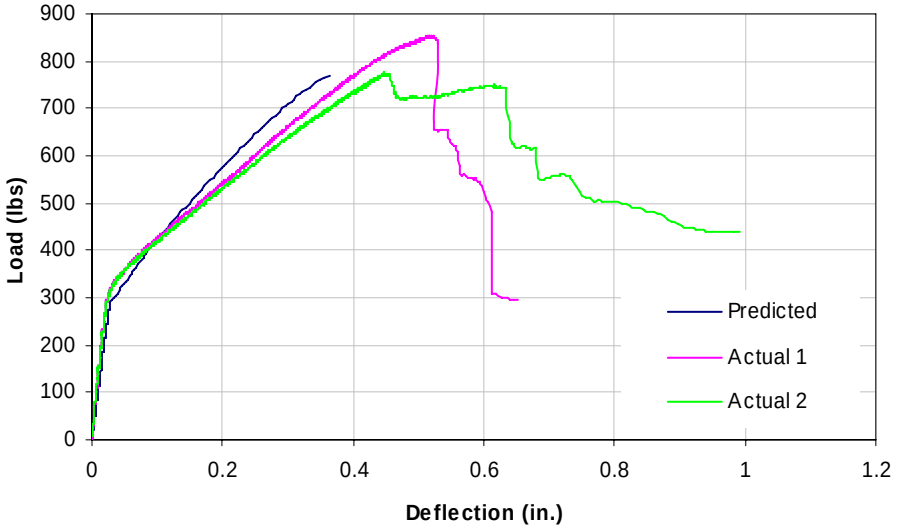

Figure 4.17 – Load-deflection curve for 1/16-200 7 day

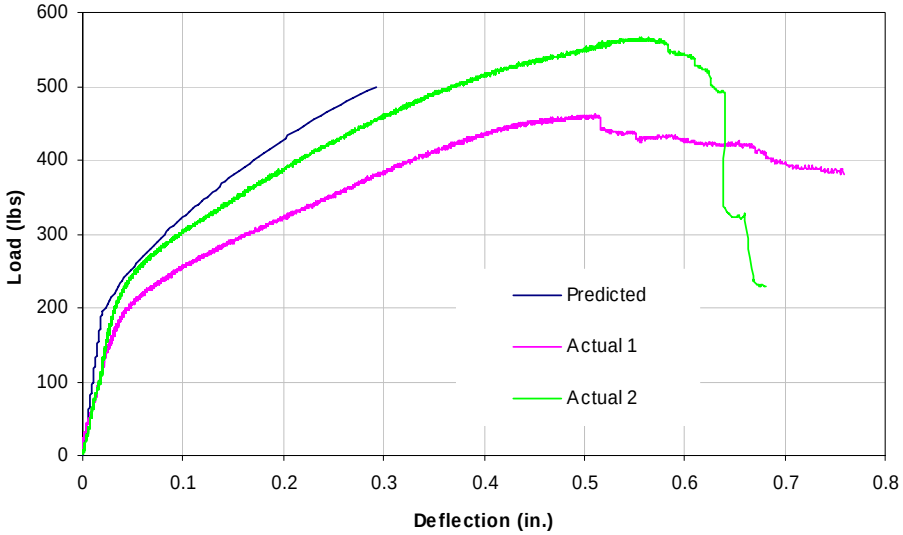

Figure 4.18 – Load-deflection curve for 3/64-150 2 day

4.5 STEEL FIBERS VERSUS NITINOL FIBERS

The samples made with steel fibers were not a very good comparison to the samples with Nitinol fibers. Because the steel fibers were glued together, the concrete-fiber mix had to turn in the concrete mixer while the glue dissolved and the fibers mixed in. Because of this, the air content of the concrete was doubled in these samples as seen in Table 4.7. Figure 4.19 compares the SMA fiber and steel fiber force-displacement curves. The steel fiber reinforced samples had no prestressing in them, so as expected, the force when the sample first cracks is higher for the SMA sample. There is little difference in the post cracking behavior of the two samples.

Table 4.7– Air Content of Fiber Samples

Specimen	Air Content
Normal Concrete (MOR)	6.13%
SF1	13.57%
SF2	12.37%
0.04 F1	6.11%
0.04 F2	5.00%
0.075 F1 & F2	6.61%

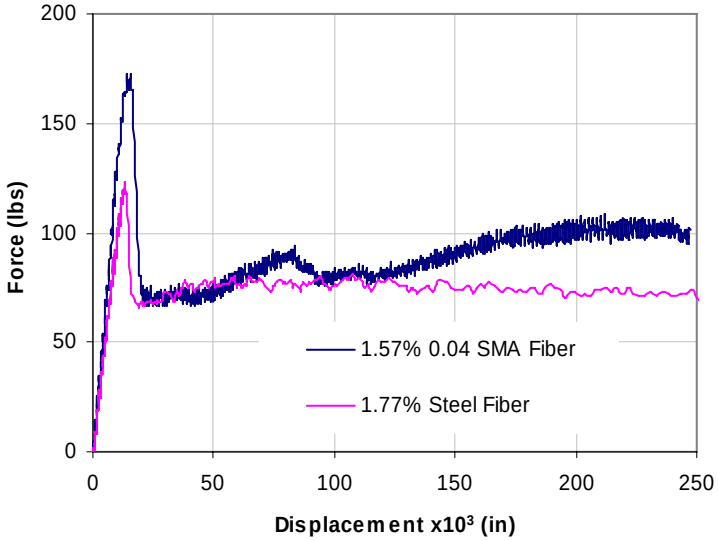

Figure 4.19 – 0.04 SMA Fiber and Steel Fiber Force-Displacement Curves

4.6 CRACK CLOSURE

The ability of the Nitinol to close cracks upon reheating was examined. Each specimen was heated with a heat gun after its initial break. The heat gun allowed the specimen to remain in the test machine and the recovery to be actively measured while the specimen was being heated. Without removing the sample from the test machine, it was reloaded. The sample was then reheated in an oven to ensure the entire sample reached a temperature above A_f. Once cool, the samples were loaded a second time. Table 4.8 shows the amount of recovery the specimen regained when under the heat gun. All the samples showed some recovery and as expected, increasing the amount of Nitinol in the sample, increases amount of recovery that occurs. The 0.075 inch diameter alloy X specimens showed the most recovery, and when reheated in the oven, little if any additional recovery was noticed as seen in Figure 4.21. The 0.04 inch diameter wire recovered almost twice as much when placed in the oven as it initially did with the heat gun as seen in Figure 4.20. This is due the fact that the 0.075 inch alloy X stays in its austenite phase once it is heated the first time. The 0.04 inch Alloy M wire is martensite at room temperature, so it goes through a phase change every time it is heated and results in more crack closure.

Table 4.8 – Recovery and Crack Closure when Nitinol is Reheated

Specimen	Average Recovery (in)	Percent Recovered	% Nitinol
.04 Straight	0.0215	17.5%	2.01
.04 Fiber 1	0.0200	8.9%	1.57
.04 Fiber 2	0.0065	2.3%	0.47
.075 Straight	0.0340	24.5%	1.19

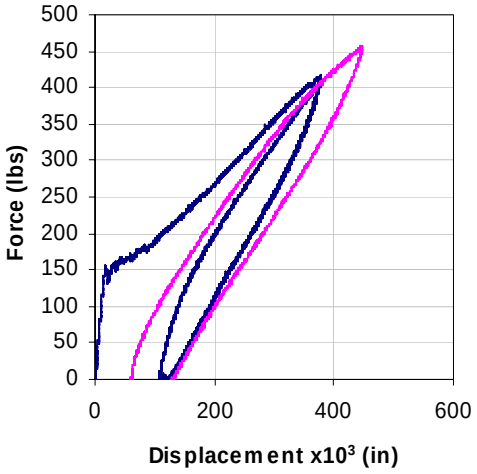

Figure 4.20 – Recovery of 0.04" Wire

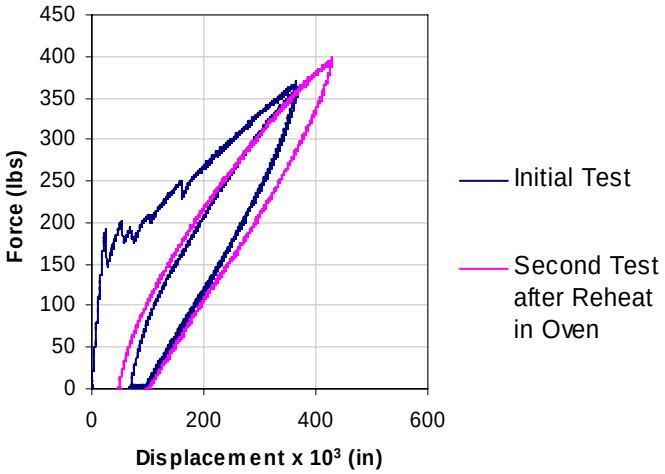

Figure 4.21 – Recovery of 0.075" Wire

Chapter 5
Summary and Conclusions

5.1 SUMMARY

The purpose of this project was to study what factors effect prestressing and if shape memory alloys such as Nitinol be used to prestress concrete. Prestressing with steel cables limits the size and shape of the member which can be prestressed. If a fiber could be used instead of a straight tendon, then thin or curved shaped members could be easily prestressed. While this study concludes that Nitinol does induce a prestressing force, there is a lot of variability in the Nitinol samples. Further research is needed to find a more effective way to prestress with Nitinol. Looking at it from a cost perspective, the steel cables are less then 15 percent of the price of the Nitinol. The steel cables also hold higher prestressing loads and reduce the defection in the sample. While the Nitinol can be used for a larger variety of shapes, it does not seem like a realistic method of prestressing concrete.

5.2 CONCLUSIONS

5.2.1 Force at Initial Crack

The difference in the force required to crack the beams were analyzed, and the load-displacement curves produced by the different prestressed beams were compared. Changing the prestressing force, released date, prestressing tendon diameter, and the prestressing tendon material produced the following conclusions:

1. Increasing the prestressing force in the tendons typically increases the force required to crack the sample.
2. Varying the release date has no noticeable effect on the force required to crack the member, but the elastic shortening is reduced as the concrete becomes stronger.
3. The cable size does not affect the bending stress required to crack a sample; it is the force in the cable which is important.
4. Nitinol can be used to prestress concrete.

5.2.2 Elastic Shortening and Concrete Shrinkage

Each sample was measured before and after the prestressing force was applied. Analysis of the amount of elastic shortening in the different sample yielded the following conclusions:

1. Increasing E_c decreases the amount of elastic shortening that occurs in a sample.
2. When E_s increases, so does the amount of elastic shortening in a sample.

5.2.3 Crack Closure with Nitinol

When reheated, the cracks in the concrete only closed between 5 and 25 percent depending on the amount of Nitinol in the sample. Increasing the amount of Nitinol wires or fibers in each sample would result in more complete crack closure.

5.3 RECOMMENDATIONS FOR FUTURE WORK

While prestressing concrete with steel cables went very smoothly, prestressing concrete with Nitinol had a number of challenges. It is possible to prestress concrete using Nitinol wires and fibers, but more research is needed. Some of the ideas for future work include:

1. To reduce material cost, a type three shape memory alloy (SMA) could be used without prestraining it. The force resulting from the phase change is about three times larger then the force from prestraining the sample. For this project, the 0.075 inch diameter Nitinol wire was a type three SMA, so it remained austenite at room temperature and it was prestrained. A large portion of the material cost went to fees to prestrain the wire. Without the prestraining, the prestressing force in the wire would be about 25 percent less and it would cost half to a third as much.
2. A larger number of smaller diameter fibers is better then a low number of larger ones.
3. The bondage between the Nitinol and the concrete can be improved. While the hooks at the ends of the fibers and straight wires did not pull out, the graphs indicate that some slipping did occur along the length of the sample.

4. A different method of anchoring the fibers could be explored. It was very evident that the hooks in the larger wire were trying to straighten and adding undesired stress to the sample. Bending the wire in a hook also resulted in making a brittle spot in the wire due to the Nitinol's strain hardening properties. If prestraining is not used, the wires could be welded then cooled below their martensite finish temperature.

References

ASTM C1399 (2004). "Test Method for Obtaining Average Residual-Strength of Fiber Reinforced Concrete, ASTM International, West Conshohocken, PA, 6 pp.

ASTM C1609 (2005). "Standard Test Method for Flexural Performance of Fiber Reinforced Concrete (Using Beam with Third-Point Loading)," ASTM International, West Conshohocken, PA, 8 pp.

Chen, K.; Pfister, Nick; and Schmigt, Matthem (2001) "Mate 375 kinetics of Materials Laboratory"

Deng, Z.; Li, Q.; Jiu, A.; and Li, L. (2003). "Behavior of Concrete Driven by Uniaxially Embedded Shape Memory Alloy Actuators," ASCE Journal of Engineering Mechanics, V. 129, No. 6, pp. 697-703.

Deng, Z.; Li, Q.; and Sun, H. (2006). "Behavior of Concrete Beam with Embedded Shape Memory Alloy Wires," EngineeringStructures, V. 28, pp. 1691-1697.

El-Tawil, S., and Ortega-Rosales, J. (2004). "Prestressing Concrete Using Shape Memory Alloy Tendons," *ACI Structural Journal*, Vol. 101, No. 6, pp. 846-851.

Freed, Y.; Aboudi, J.; and Gilat, R. (2007). "Thermomechanically Micoromechanical Modeling of Prestressed Concrete Reinforced with Shape Memory Alloy Fibers," Smart Materials and Structures, V. 16, pp. 717-727.

"Fundamental Characteristics of Nickel- Titanium Shape Memory Alloy (2000)," Oulu University Library, 26 July 2007 <http://herkules.oulu.fi/isbn9514252217/html/x317.html>.

Hsu, Jer-Wen. (1996) "Structural Repair and Retrofit Systems Based on Shape-Memory Alloys."

James Instruments Inc. "E-Meter Resonant Frequency Tester C-4959 Mark II," Product Manual.

Kotamala, S. (2004) "Prestressing of Simply Supported Concrete Beam with Nitinol Shape Memory Alloy," MS thesis, The University of Toledo, OH, 64 pp.

Krstulovic-Opara, N., and Naaman, A.E. (2000). "Self-Stressing Fiber Composites," *ACI Structural Journal*, Vol. 97, No. 2, pp. 335-344.

Li, L.; Li, Q.; and Zhang, F. (2007). "Behavior of Smart Concrete Beams with Embedded Shape Memory Alloy Bundles," Journal of Intelligent Material Systems and Structures, v. 18, pp. 1003-1014.

Lydon, F.D.; and Balendran, R.V. (1986). "Some observations on elastic properties of plain concrete," *Cement and Concrete Research*, Vol. 16, No. 3, pp.314-324.

Maji, A.K., and Negret, I. (1998). "Smart Prestressing with Shape-Memory Alloy," *Journal of Engineering Mechanics*," Vol. 124, No. 10, pp. 1121-1128.

Moser, K.; Bergamini, A.; Christen, R.; Czaderski, C. (2005). "Feasibility of Concrete Prestressed by Shape Memory Alloy Short Fibers," *Materials and Structures*, Vol. 38, June 2005, pp. 593-600.

Naaman, A.E. (2004). Prestressed Concrete Analysis and Design: Fundamentals, 2nd Edition, Techno Press 3000, publisher, 1072 pp.

NDC. (2005), "Nitinol Facts," Nitinol Devices and Components, 21 July 2008 <www.nitinol.com>.

Neville, A.M. (1956). "The influence of size of concrete tests cubes on mean strength the standard deviation," *Mag. Concr. Res*., Vol. 8, No. 23, pp. 101-110.

"Nitinol/Flexinal Wire," Images SI Inc., 27 July 2007 <www.imagesco.com/articles/nitinol/04.html>.

Pan, Q., and Cho, C. (2007). "The Investigation of a Shape Memory Alloy Micro-Damper for MEMS Applications," Sensors, V. 7, pp. 1887-1900.

Pelton, A.; Russell, S.; DiCello, J. (2003). "The Physical Metallurgy of Nitinol for Medical Applications," Journal of Medicine, May 2003, pp. 33-37.

Saiidi, M.; Sadrossadat-Zadeh, M.; Ayoub, C.; and Itani, A. (2007). "Pilot Study of Behavior of Concrete Beams Reinforced with Shape Memory Alloys," ASCE Journal of Materials in Civil Engineering, V. 19, No. 6, pp. 454-461.

Somayaji, Shan. (2001). Civil Engineering Materials, 2nd Edition, Prentice Hall, publisher, 477pp.

W. R. Grace and Co. (2002), "Polar Set Product Information," Grace Construction Products, <www.graceconstruction.com>.

W. R. Grace and Co. (2003), "ADVA Cast 500," Grace Construction Products, <www.graceconstruction.com>.

Appendix : A

Test Specimens

	2 day		7 day		14 day	
3_64_150	1	2	3	4	5	6
Comp (lbs)	28230	22420	42260	44280	41110	46830
fc' (psi)	3993.728	3171.781	5978.567	6264.339	5815.875	6625.09
Conv to 4x8 (psi)	3218.622	2482.322	4996.64	5252.634	4850.901	5575.795
Initial Force (lbs)	2400	2400	2400	2400	2400	2400
Theoretical ES (psi)	15191.28	15784.27	17329.58	16687.11	10051.65	10166.82
Theoretical S (psi)	1858.085	1858.085	1858.085	1858.085	1858.085	1858.085
Theoretical ES,S (lbs)	10.897	11.276	12.263	11.853	7.612	7.685
Exp ES, S, & C (in)	0.00575	0.00575	0.00575	0.00575	0.00575	0.00575
Exp ES, S, & C (lbs)	10.47	10.47	10.47	10.47	10.47	10.47
Theo Relaxation (K=10) (lbs)	26.38255	26.38255	34.92024	34.92024	39.64409	39.64409
Exp Relaxation (lbs)	480	480	480	480	480	480
Force Applied (psi)	1909.53	1909.53	1909.53	1909.53	1909.53	1909.53
Exp MOR (psi)	328.6662	328.6662	554.1562	554.1562	562.6915	562.6915
Theo MOR (psi)	640.678	640.678	859.039	859.039	866.442	866.442
Theo MOR (lbs)	152.5544	143.6462	189.4894	203.4104	197.8536	190.9773
L (in)	24.375	24	23.75	23.625	24	23.6875
t1 (in)	1.01	0.9995	0.964	1.0425	0.9835	1.007
t2 (in)	1.031	0.9715	1.025	1.01	1.04	0.961
t3 (in)	1.0345	1.0315	1.0205	1.0435	0.9715	1.016
t4 (in)	1.0145	0.999	0.9705	1.018	1.0565	0.9715
b1 (in)	4.09	4.02	4.0305	4.0325	3.9835	4.0805
b2 (in)	4.109	4.0455	3.9905	4.026	4.0295	4.034
t_ave (in)	1.0225	1.000375	0.995	1.0285	1.012875	0.988875
b_ave (in)	4.0995	4.03275	4.0105	4.02925	4.0065	4.05725
P_computer (lbs)	566.1	461.6	462.6	648	670	660
Crack (lbs)	215	190	215	270	225	270
P load cell (lbs)	566.5	418.2	441.1	644.7	665.7	654.7
Stress (psi)	2379.112	1865.218	1999.7	2722.685	2915.239	2970.3
Theoretical Crack (lbs)	186.732	179.815	227.792	240.326	235.942	228.931
Actual Crack (lbs)	215.4	146.6	193.5	266.7	220.7	264.7
Crack Percent Error (%)	-15.35	18.47	15.05	-10.97	6.46	-15.62
Ave Percent Error (%)		1.56		2.04		-4.58
Stress Crack (psi)	904.6085	653.8521	877.2205	1126.322	966.4914	1200.914
n (Hz)	186	207	192	200	248	250
W (g)	3422.7	3300.7	3253.1	3314.5	3304.1	3267.5
L (m)	0.619133	0.609607	0.603257	0.600082	0.609607	0.60167
t (m)	0.025972	0.02541	0.025273	0.026124	0.025727	0.025118
b (m)	0.104129	0.102433	0.101868	0.102344	0.101766	0.103055
W (kg)	3.4227	3.3007	3.2531	3.3145	3.3041	3.2675
K (m)	0.007498	0.007335	0.007296	0.007542	0.007427	0.007251
K/L	0.01211	0.012033	0.012094	0.012568	0.012183	0.012052
T	1.040467	1.040165	1.040406	1.042275	1.040756	1.040238
C	128108.2	132703.4	131450.3	116814.4	128761.4	131301.6
Dynamic Ec (psi)	2200187	2722178	2286384	2246272	3795158	3889140
Static Ec (psi)	1826155	2259408	1897699	1864405	3149981	3227986

Ave Comp (psi)		2850.472		5124.637		5213.348
Ave Break Stress (psi)		2122.165		2361.192		2942.77
Ave Crack Stress (psi)		779.2303		1001.771		1083.703
Ave Dynamic Ec (psi)		2461182		2266328		3842149
Ave Static Ec (psi)		2042781		1881052		3188984

	2 day		7 day		14 day	
3_64_200	1	2	3	4	5	6
Comp (lbs)	29770	23210	60250	39110	47930	43260
fc' (psi)	4211.593	3283.543	8523.631	5532.933	6780.7079	6120.0381
Conv to 4x8 (psi)	3413.785	2582.438	7276.509	4597.442	5715.1982	5123.3701
Initial Force (lbs)	3160	3160	3160	3160	3160	3160
Theoretical ES (psi)	13740.75	14037.93	11825.19	11973.47	12837.828	13416.748
Theoretical S (psi)	1858.085	1858.085	1858.085	1858.085	1858.0854	1858.0854
Theoretical ES,S (lbs)	9.970	10.159	8.745	8.840	9.392	9.762
Exp ES, S, & C (in)	0.00595	0.00595	0.00595	0.00595	0.00595	0.00595
Exp ES, S, & C (lbs)	10.84	10.84	10.84	10.84	10.84	10.84
Theo Relaxation (lbs)	138.267	138.267	183.0117	183.0117	207.76873	207.76873
Exp Relaxation (lbs)	560	560	560	560	560	560
Force Applied (psi)	2589.16	2589.16	2589.16	2589.16	2589.16	2589.16
Exp MOR (psi)	343.785	343.785	503.0871	503.0871	582.44495	582.44495
Theo MOR (psi)	657.060	657.060	924.621	924.621	883.389	883.389
Theo MOR (lbs)	153.3772	150.3162	213.6066	211.5577	210.76856	191.71126
L (in)	23.625	23.875	23.875	24	24.125	23
t1 (in)	0.997	1.0295	1.0115	1.0355	1.024	0.9905
t2 (in)	1.0205	1.0005	1.016	1.0195	1.038	0.985
t3 (in)	0.9985	1.0205	1.0205	1.014	1.038	1.015
t4 (in)	1.0225	0.993	1.0195	1.01	1.0295	0.935
b1 (in)	4.116	4.018	4.009	4.0045	4.0185	4.026
b2 (in)	4.128	4.0415	4.034	3.9165	4.0405	4.086
t_ave (in)	1.009625	1.010875	1.016875	1.01975	1.032375	0.981375
b_ave (in)	4.122	4.02975	4.0215	3.9605	4.0295	4.056
P_computer (lbs)	667.8	635.7	611.81	624.3	694	720.6
Crack (lbs)	255	190	245	265	285	280
P load cell (lbs)	668.6	629.3	625.1	599.5	693.1	721.3
Stress (psi)	2864.249	2750.789	2705.819	2620.138	2904.9742	3323.69
Theoretical Crack (lbs)	225.476	224.055	262.493	261.792	287.465	267.564
Actual Crack (lbs)	255.8	183.6	258.29	240.2	284.1	280.7
Crack Percent Error (%	-13.45	18.06	1.60	8.25	1.17	-4.91
Ave Percent Error (%)		-13.45		4.92		-1.87
Stress Crack (psi)	1095.834	802.5501	1118.039	1049.804	1190.7419	1293.4421
n (Hz)	273	221	255	274	248	269
W (g)	3275.5	3280.7	3324	3323.2	3341.3	3145.5
L (m)	0.600082	0.606432	0.606432	0.609607	0.6127825	0.5842071
t (m)	0.025645	0.025677	0.025829	0.025902	0.0262226	0.0249272
b (m)	0.1047	0.102357	0.102147	0.100598	0.1023505	0.1030237
W (kg)	3.2755	3.2807	3.324	3.3232	3.3413	3.1455
K (m)	0.007403	0.007412	0.007456	0.007477	0.00757	0.0071961
K/L	0.012337	0.012223	0.012296	0.012266	0.0123536	0.0123177
T	1.041362	1.040912	1.041198	1.041081	1.0414269	1.0412852
C	120604.8	126797.1	124855.7	127680	122886.13	123136.27
Dynamic Ec (psi)	4270268	2946783	3914150	4620281	3662768.8	4065070.2
Static Ec (psi)	3544322	2445830	3248744	3834833	3040098.1	3374008.3

Ave Comp (psi)		2998.112		4597.442		5419.2841
Ave Break Stress (psi)		2807.519		2662.979		3114.3321
Ave Crack Stress (psi)		949.1922		1083.921		1242.092
Ave Dynamic Ec (psi)		3608525		4267215		3863919.5
Ave Static Ec (psi)		2995076		3541789		3207053.2

	14 day		28 day	
3_64_200B	1	2	3	4
Comp (lbs)	44360	56570	60720	54440
fc' (psi)	6275.656	8003.018	8590.123	7701.685
Conv to 4x8 (psi)	5262.773	6810.143	7336.072	6540.209
Initial Force (lbs)	3140	3140	3140	3140
Theoretical ES (psi)	19995.07	19943.01	10361.9	10307.99
Theoretical S (psi)	1858.085	1858.085	1858.085	1858.085
Theoretical ES,S (lbs)	13.967	13.934	7.810	7.776
Exp ES, S, & C (in)	0.0016	0.0016	0.0016	0.0016
Exp ES, S, & C (lbs)	2.91	2.91	2.91	2.91
Theo Relaxation (lbs)	134.6847	134.6847	178.2701	178.2701
Exp Relaxation (lbs)	560	560	560	560
Force Applied (psi)	2577.09	2577.09	2577.09	2577.09
Exp MOR (psi)	641.1665	641.1665	688.6081	688.6081
Theo MOR (psi)	932.336	932.336	999.546	999.546
Theo MOR (lbs)	230.7061	236.8031	248.5313	249.2103
L (in)	24.5	24.25	24	23.625
t1 (in)	1.0085	1.0735	1.095	1.0855
t2 (in)	1.0655	1.0765	1.045	1.0455
t3 (in)	1.0305	1.0725	1.085	1.05
t4 (in)	1.063	1.044	1.0015	1.035
b1 (in)	4.077	4.0105	4.001	4.048
b2 (in)	4.1295	4.0265	4.0165	4.0315
t_ave (in)	1.041875	1.066625	1.056625	1.054
b_ave (in)	4.10325	4.0185	4.00875	4.03975
P_computer (lbs)	408.9	403.6	618.5	653.8
Crack (lbs)	310	318	350	313
P load cell (lbs)	409.6	404.5	600.8	649
Stress (psi)	1655.287	1592.588	2416.305	2603.044
Theoretical Crack (lbs)	307.823	315.559	322.497	322.589
Actual Crack (lbs)	310.7	318.9	332.3	308.2
Crack Percent Error (%)	-0.93	-1.06	-3.04	4.46
Ave Percent Error (%)		-1.00		0.71
Stress Crack (psi)	1255.609	1255.566	1336.448	1236.145
n (Hz)	198	197	291	281
W (g)	3568.5	3601	3607.6	3472.8
L (m)	0.622308	0.615957	0.609607	0.600082
t (m)	0.026464	0.027093	0.026839	0.026772
b (m)	0.104224	0.102071	0.101823	0.102611
W (kg)	3.5685	3.601	3.6076	3.4728
K (m)	0.00764	0.007821	0.007748	0.007729
K/L	0.012276	0.012698	0.01271	0.012879
T	1.041122	1.042792	1.04284	1.043518
C	122930.9	113623.8	113583.6	108386.4
Dynamic Ec (psi)	2494392	2303100	5032776	4310770
Static Ec (psi)	2070346	1911573	4177204	3577939

Ave Comp (psi)		6036.458		6540.209
Ave Break Stress (psi)		1623.938		2509.674
Ave Crack Stress (psi)		1255.588		1286.297
Ave Dynamic Ec (psi)		2398746		4671773
Ave Static Ec (psi)		1990959		3877572

	2 day		7 day		14 day	
1_16_10	1	2	3	4	5	6
Comp (lbs)		28120	48920	58030	60050	56570
fc' (psi)		3978.166	6920.764	8209.566	8495.337	8003.018
Conv to 4x8 (psi)	3204.681	3204.681	5840.661	6995.169	7251.163	6810.143
Initial Force (lbs)	160	160	160	160	160	160
Theoretical ES (psi)	826.4136	833.9185	545.7904	557.1354	531.4125	529.4674
Theoretical S (psi)	1522.122	1522.122	1522.122	1522.122	1522.122	1522.122
Theoretical ES,S (lbs)	2.403	2.410	2.115	2.127	2.101	2.099
Exp ES, S, & C (in)	0.00095	0.00095	0.00095	0.00095	0.00095	0.00095
Exp ES, S, & C (lbs)	1.73	1.73	1.73	1.73	1.73	1.73
Theo Relaxation (lbs)	0	0	0	0	0	0
Exp Relaxation (lbs)	0	0	0	0	0	0
Force Applied (psi)	158.27	158.27	158.27	158.27	158.27	158.27
Exp MOR (psi)	364.8028	364.8028	677.1288	677.1288	734.4133	734.4133
Theo MOR (psi)	679.319	679.319	961.343	961.343	1006.188	1006.188
Theo MOR (lbs)	148.4296	148.723	218.2008	211.3116	231.586	231.1742
L (in)	24	23.875	23.625	24	23.875	23.785
t1 (in)	0.9195	0.9765	1.017	0.987	0.9855	1.018
t2 (in)	0.988	0.99	1.012	0.973	1.0405	0.975
t3 (in)	0.997	0.9955	0.996	1.031	0.982	1.049
t4 (in)	1.023	1.009	0.995	0.983	1.042	0.986
b1 (in)	4.0905	4.0205	4.0565	4.011	4.023	4.061
b2 (in)	4.0685	3.9765	4.0335	4.006	4.0595	4.0955
t_ave (in)	0.981875	0.99275	1.005	0.9935	1.0125	1.007
b_ave (in)	4.0795	3.9985	4.045	4.0085	4.04125	4.07825
P_computer (lbs)	673	635.67	711.5	742.15	845.5	818.5
Crack (lbs)	105	145	185	175	215	185
P load cell (lbs)	678.1	574.2	739.7	701.2	835.8	812.2
Stress (psi)	3103.465	2622.762	3258.948	3190.045	3631.358	3535.108
Theoretical Crack (lbs)	88.342	88.595	162.528	157.574	177.937	177.588
Actual Crack (lbs)	110.1	83.53	213.2	134.05	205.3	178.7
Crack Percent Error (%	-24.63	5.72	-31.18	14.93	-15.38	-0.63
Ave Percent Error (%)		-9.46		-8.12		-8.00
Stress Crack (psi)	503.8955	381.5383	939.3102	609.8481	891.9811	777.7934
n (Hz)	214	179	256	240	257	250
W (g)	3357.6	3319.7	3307.3	3337.2	3379.3	3344.1
L (m)	0.609607	0.606432	0.600082	0.609607	0.606432	0.604146
t (m)	0.02494	0.025216	0.025527	0.025235	0.025718	0.025578
b (m)	0.103621	0.101563	0.102744	0.101817	0.102649	0.103589
W (kg)	3.3576	3.3197	3.3073	3.3372	3.3793	3.3441
K (m)	0.0072	0.007279	0.007369	0.007285	0.007424	0.007384
K/L	0.01181	0.012004	0.012281	0.01195	0.012243	0.012222
T	1.039295	1.040051	1.041138	1.039841	1.040989	1.040909
C	138622.2	134804.2	124578.5	136254.5	125837.8	125312.8
Dynamic Ec (psi)	3091556	2079679	3916375	3798774	4073728	3798766
Static Ec (psi)	2565991	1726133	3250591	3152983	3381194	3152976
Ave Comp (psi)		3204.681		6417.915		7030.653
Ave Break Stress (psi)		2863.113		3224.497		3583.233
Ave Crack Stress (psi)		442.7169		774.5792		834.8873
Ave Dynamic Ec (psi)		2585617		3857575		3936247
Ave Static Ec (psi)		2146062		3201787		3267085

	2 day		7 day		14 day	
1_16_200	1	2	3	4	5	6
Comp (lbs)	31800	33810	49630	44750	54740	54890
fc' (psi)	4498.78	4783.137	7021.209	6330.83	7744.1259	7765.347
Conv to 4x8 (psi)	3671.047	3925.774	5930.639	5312.197	6578.2279	6597.237
Initial Force (lbs)	3200	3200	3200	3200	3200	3200
Theoretical ES (psi)	13064.96	13140.55	9495.533	9308.003	9325.46	9381.617
Theoretical S (psi)	1522.122	1522.122	1522.122	1522.122	1522.1216	1522.122
Theoretical ES,S (lbs)	14.923	15.000	11.271	11.079	11.097	11.155
Exp ES, S, & C (in)	0.0028	0.0028	0.0028	0.0028	0.0028	0.0028
Exp ES, S, & C (lbs)	5.10	5.10	5.10	5.10	5.10	5.10
Theo Relaxation (lbs)	0	0	0	0	0	0
Exp Relaxation (lbs)	640	640	640	640	640	640
Force Applied (psi)	2554.90	2554.90	2554.90	2554.90	2554.90	2554.90
Exp MOR (psi)	424.4237	424.4237	601.754	601.754	693.0626	693.0626
Theo MOR (psi)	739.575	739.575	899.713	899.713	973.978	973.978
Theo MOR (lbs)	176.2814	176.8346	217.3827	224.4207	245.61331	241.1616
L (in)	24.625	23.625	24.375	23.75	23.75	23.25
t1 (in)	1.043	1.033	1.0425	1.0505	1.073	1.0465
t2 (in)	1.0035	1.002	1.071	1.0445	1.036	1.046
t3 (in)	0.998	1.052	1.0285	1.08	1.0795	1.0475
t4 (in)	1.0375	1.0315	1.029	1.046	1.0695	1.066
b1 (in)	4.1405	4.0915	3.9995	4.0415	4.0205	4.052
b2 (in)	4.099	4.028	4	4.0225	3.991	4.01
t_ave (in)	1.0205	1.029625	1.04275	1.05525	1.0645	1.0515
b_ave (in)	4.11975	4.05975	3.99975	4.032	4.00575	4.031
P_computer (lbs)	535.91	398.257	775.646	854.533	1043.33	1009.33
Crack (lbs)	290	272	315	316	333	358
P load cell (lbs)	512.2	375.6	765.3	845.6	1044.2	1007.2
Stress (psi)	2148.895	1570.871	3167.459	3390.051	4140.7692	4067.775
Theoretical Crack (lbs)	246.012	247.625	293.398	299.880	325.867	320.854
Actual Crack (lbs)	266.29	249.343	304.654	307.067	333.87	355.87
Crack Percent Error (%	-8.24	-0.69	-3.84	-2.40	-2.46	-10.91
Ave Percent Error (%)		-4.47		-3.12		-6.68
Stress Crack (psi)	1117.199	1042.827	1260.916	1231.046	1323.9596	1437.251
n (Hz)	227	223	260	314	279	288
W (g)	3464.5	3372.9	3557.7	3509.2	3510.5	3454.5
L (m)	0.625483	0.600082	0.619133	0.603257	0.6032573	0.590557
t (m)	0.025921	0.026153	0.026486	0.026804	0.0270386	0.026708
b (m)	0.104643	0.103119	0.101595	0.102414	0.1017473	0.102389
W (kg)	3.4645	3.3729	3.5577	3.5092	3.5105	3.4545
K (m)	0.007483	0.00755	0.007646	0.007738	0.0078056	0.00771
K/L	0.011964	0.012581	0.01235	0.012827	0.0129391	0.013056
T	1.039893	1.04233	1.041412	1.043307	1.0437573	1.044226
C	132142.7	115563.3	123913.5	109913.8	107821.47	104341.9
Dynamic Ec (psi)	3421553	2811388	4322375	5515786	4273369.3	4336272
Static Ec (psi)	2839889	2333452	3587571	4578102	3546896.5	3599106
Ave Comp (psi)		3798.41		5621.418		6587.733
Ave Break Stress (psi)		1859.883		3278.755		4104.272
Ave Crack Stress (psi)		1080.013		1245.981		1380.605
Ave Dynamic Ec (psi)		3116470		4322375		4304821
Ave Static Ec (psi)		2586670		3587571		3573001

	2 day		7 day		14 day	
1_16_240	1	2	3	4	5	6
Comp (lbs)	32540	33470	51620	50610	56370	59840
fc' (psi)	4603.468	4735.036	7302.736	7159.85	7974.723682	8465.628
Conv to 4x8 (psi)	3764.827	3882.686	6182.831	6054.834	6784.797474	7224.55
Initial Force (lbs)	3840	3840	3840	3840	3840	3840
Theoretical ES (psi)	25428.15	25895.31	21620.08	21549.93	24573.22767	24562.49
Theoretical S (psi)	1522.122	1522.122	1522.122	1522.122	1522.121606	1522.122
Theoretical ES,S (lbs)	27.570	28.048	23.674	23.603	26.696	26.685
Exp ES, S, & C (in)	0.00205	0.00205	0.00205	0.00205	0.00205	0.00205
Exp ES, S, & C (lbs)	3.73	3.73	3.73	3.73	3.73	3.73
Theo Relaxation (lbs)	0	0	0	0	0	0
Exp Relaxation (lbs)	960	960	960	960	960	960
Force Applied (psi)	2876.27	2876.27	2876.27	2876.27	2876.27	2876.27
Exp MOR (psi)	426.9451	426.9451	648.953	648.953	731.9959528	731.996
Theo MOR (psi)	742.038	742.038	938.676	938.676	1004.327	1004.327
Theo MOR (lbs)	175.9888	171.5471	219.7067	220.4219	230.0291793	228.9644
L (in)	23.75	23.875	24.25	24	23.875	24
t1 (in)	1.0065	1.017	1.036	1.033	1.023	0.969
t2 (in)	1.04	1.006	1.033	1.0325	0.9695	1.031
t3 (in)	1.018	1.0105	1.022	1.0215	1.0245	1.019
t4 (in)	1.028	1.029	1.0175	1.0215	1.0315	1.009
b1 (in)	4.038	4.0505	4.0055	4.002	4.0555	4.061
b2 (in)	4.1185	4.018	3.9815	4.011	3.9935	4.0325
t_ave (in)	1.023125	1.015625	1.027125	1.027125	1.012125	1.007
b_ave (in)	4.07825	4.03425	3.9935	4.0065	4.0245	4.04675
P_computer (lbs)	442.46	324.95	640.96	812	875	830.64
Crack (lbs)	305	240	220	315	305	273
P load cell (lbs)	426.2	325.8	643.1	812.7	871.2	826.7
Stress (psi)	1797.027	1409.269	2747.582	3460.916	3803.733974	3626.228
Theoretical Crack (lbs)	264.746	260.992	316.021	316.516	329.385	296.862
Actual Crack (lbs)	288.74	240.85	222.14	315.7	301.2	269.06
Crack Percent Error (%)	-9.06	7.72	29.71	0.26	8.56	9.37
Ave Percent Error (%)		-0.67		0.26		8.96
Stress Crack (psi)	1217.442	1041.813	949.0716	1344.421	1315.065052	1448.694
n (Hz)	180	181	187	196	191	170
W (g)	3386.4	3331.8	3450.5	3480.2	3398.3	3366.1
L (m)	0.603257	0.606432	0.615957	0.609607	0.606432374	0.609607
t (m)	0.025988	0.025797	0.026089	0.026089	0.025708288	0.025578
b (m)	0.103589	0.102471	0.101436	0.101766	0.102223543	0.102789
W (kg)	3.3864	3.3318	3.4505	3.4802	3.3983	3.3661
K (m)	0.007502	0.007447	0.007532	0.007532	0.007421561	0.007384
K/L	0.012436	0.01228	0.012227	0.012355	0.012238069	0.012113
T	1.041754	1.041138	1.040929	1.041432	1.040971131	1.040478
C	119050.6	124914	127811.1	123556.4	126499.8969	129690.3
Dynamic Ec (psi)	1894535	1977585	2236771	2395903	2274607.216	1829870
Static Ec (psi)	1572464	1641395	1856520	1988600	1887923.989	1518792
Ave Comp (psi)		3823.756		6118.833		7004.674
Ave Break Stress (psi)		1603.148		3104.249		3714.981
Ave Crack Stress (psi)		1129.627		1344.421		1381.88
Ave Dynamic Ec (psi)		1936060		2316337		2052238
Ave Static Ec (psi)		1606930		1922560		1703358

	2 day		7 day		14 day	
Fiber _1.77	1	2	3	4	5	6
Comp (lbs)	13770	13840	21550	21790	33890	34960
fc' (psi)	1948.0565	1957.959	3048.701	3082.654	4794.454	4945.828
Conv to 4x8 (psi)	1386.109	1394.98	2372.067	2402.482	3935.912	4071.513
Initial Force (lbs)						
Theoretical ES (psi)						
Theoretical S (psi)						
Theoretical ES,S (lbs)						
Exp ES, S, & C (in)	0.00095	0.00095	0.00095	0.00095	0.00095	0.00095
Exp ES, S, & C (lbs)						
Theo Relaxation (lbs)						
Exp Relaxation (lbs)						
Force Applied (psi)	0.00	0.00	0.00	0.00	0.00	0.00
Exp MOR (psi)	173.43099	173.431	280.6506	280.6506	444.7948	444.7948
Theo MOR (psi)	447.480	447.480	586.317	586.317	759.299	759.299
Theo MOR (lbs)	106.81774	107.96	164.0062	146.7306	187.0236	205.4833
L (in)	24.0625	23.75	24.375	24	23.75	23.75
t1 (in)	1.028	1.0425	1.0215	1.0705	1.08	1.048
t2 (in)	1.012	1.04	1.0355	1.0455	1.038	1.0175
t3 (in)	1.0295	1.0195	1.3056	1.0655	1.0395	1.3026
t4 (in)	1.0335	1.044	1.104	1.02654	1.027	1.0015
b1 (in)	4.097	4.0335	4.037	4.068	4.056	4.1165
b2 (in)	4.0705	4.051	4.039	4.0725	4.0465	4.0475
t_ave (in)	1.02575	1.0365	1.11665	1.05201	1.046125	1.0924
b_ave (in)	4.08375	4.04225	4.038	4.07025	4.05125	4.082
P_computer (lbs)	86.418	63.4	113.7	153.111	123.6	135.114
Crack (lbs)	86.418	63.4	113.7	153.111	123.6	135.114
P load cell (lbs)	84.5	63.5	113.3	159.1	131.1	143.6
Stress (psi)	353.98676	263.1991	405.0438	635.7434	532.2541	530.6285
Theoretical Crack (lbs)	41.400	41.842	78.504	70.235	109.558	120.371
Actual Crack (lbs)	84.5	63.5	113.3	159.1	131.1	143.6
Crack Percent Error (%)	-104.11	-51.76	-44.32	-126.52	-19.66	-19.30
Ave Percent Error (%)		-77.93		-85.42		-19.48
Stress Crack (psi)	353.98676	263.1991	405.0438	635.7434	532.2541	530.6285
n (Hz)	193	198	177	189	192	248
W (g)	2960.9	2907.3	3126.8	3350.6	3190.1	3189.9
L (m)	0.6111949	0.603257	0.619133	0.609607	0.603257	0.603257
t (m)	0.0260544	0.026327	0.028363	0.026721	0.026572	0.027747
b (m)	0.1037285	0.102674	0.102566	0.103386	0.102903	0.103684
W (kg)	2.9609	2.9073	3.1268	3.3506	3.1901	3.1899
K (m)	0.0075215	0.0076	0.008188	0.007714	0.007671	0.00801
K/L	0.0123062	0.012599	0.013225	0.012654	0.012716	0.013278
T	1.0412397	1.042399	1.044907	1.042619	1.042864	1.045122
C	122637.97	115592.4	100283.6	113322	112231.5	98033.74
Dynamic Ec (psi)	1961783.7	1910897	1424834	1967199	1914296	2789612
Static Ec (psi)	1628280.5	1586045	1182612	1632775	1588866	2315378

Ave Comp (psi)		1394.98		2387.274		4003.713
Ave Break Stress (psi)		308.5929		520.3936		531.4413
Ave Crack Stress (psi)		308.5929		520.3936		531.4413
Ave Dynamic Ec (psi)		1936341		1696016		2351954
Ave Static Ec (psi)		1607163		1407694		1952122

	2 day		7 day		14 day	
Fiber _2.41	1	2	3	4	5	6
Comp 2x4(lbs)	7350	7180	10760	9470	10730	11550
fc' (psi)	2339.5777	2285.465	3425.014	3014.395	3415.465	3676.479
Conv to 4x8 (psi)	1905.2735	1787.849	4260.671	3369.626	4239.949	4806.35
Initial Force (lbs)						
Theoretical ES (psi)						
Theoretical S (psi)						
Theoretical ES,S (lbs)						
Exp ES, S, & C (in)	0.00095	0.00095	0.00095	0.00095	0.00095	0.00095
Exp ES, S, & C (lbs)						
Theo Relaxation (lbs)						
Exp Relaxation (lbs)						
Force Applied (psi)	0.00	0.00	0.00	0.00	0.00	0.00
Exp MOR (psi)	223.26968	223.2697	426.089	426.089	495.8404	495.8404
Theo MOR (psi)	515.660	515.660	741.203	741.203	807.052	807.052
Theo MOR (lbs)	135.1381	125.8372	186.4238	185.7158	204.1867	199.1766
L (in)	24.25	24	24	24.25	23.0625	24.375
t1 (in)	1.047	1.0545	1.0485	1.053	1.026	1.052
t2 (in)	1.009	1.0655	1.0505	1.0465	1.076	1.0045
t3 (in)	1.055	1.015	1.076	1.0665	1.036	1.052
t4 (in)	1.035	1.026	1.051	1.046	1.098	1.0545
b1 (in)	4.7072	4.06395	4.0415	4.0815	4.0605	4.141
b2 (in)	4.0745	4.0545	4.0705	4.0535	4.061	4.0615
t_ave (in)	1.0365	1.04025	1.0565	1.053	1.059	1.04075
b_ave (in)	4.39085	4.059225	4.056	4.0675	4.06075	4.10125
P_computer (lbs)	79.5	106.56	142.15	123.72	158.82	164.115
Crack (lbs)	79.5	106.56	142.15	123.72	158.82	164.115
P load cell (lbs)	95.3	125.3	150	136.3	157.8	167.3
Stress (psi)	363.64548	513.4581	596.3851	543.9814	623.708	677.8902
Theoretical Crack (lbs)	58.512	54.485	107.168	106.761	125.449	122.371
Actual Crack (lbs)	95.3	125.3	150	136.3	157.8	167.3
Crack Percent Error (%)	-62.87	-129.97	-39.97	-27.67	-25.79	-36.72
Ave Percent Error (%)		-96.42		-33.82		-31.25
Stress Crack (psi)	363.64548	513.4581	596.3851	543.9814	623.708	677.8902
n (Hz)	170	145	179	185	190	179
W (g)	3395.5	3365.8	3445.6	3412.8	3297.7	3510.4
L (m)	0.6159575	0.609607	0.609607	0.615957	0.585795	0.619133
t (m)	0.0263274	0.026423	0.026835	0.026747	0.026899	0.026435
b (m)	0.1115289	0.103106	0.103024	0.103316	0.103144	0.104173
W (kg)	3.3955	3.3658	3.4456	3.4128	3.2977	3.5104
K (m)	0.0076003	0.007628	0.007747	0.007721	0.007765	0.007631
K/L	0.012339	0.012513	0.012708	0.012535	0.013256	0.012326
T	1.0413693	1.042057	1.042834	1.042147	1.045032	1.041318
C	113166.85	117463.9	112299.6	116597	99035.4	121533.9
Dynamic Ec (psi)	1610677.5	1205637	1798195	1975283	1710002	1982659
Static Ec (psi)	1336862.3	1000679	1492502	1639485	1419302	1645607

Ave Comp (psi)		1787.849		3815.149		4523.15
Ave Break Stress (psi)		438.5518		570.1833		650.7991
Ave Crack Stress (psi)		438.5518		570.1833		650.7991
Ave Dynamic Ec (psi)		1408157		1886739		1846330
Ave Static Ec (psi)		1168771		1565994		1532454

	Straight		Fiber1		Fiber + Steel	
0.4 SMA	1	2	3	4	5	6
Comp 2x4 (lbs)	9430	9430	21260	13070	14090	14090
fc' (psi)	3001.66223	3001.662	6767.26818	4160.31	4484.986	4484.986
Conv to 4x8 (psi)	4341.99703	4341.997	6856.26316	6856.263	7560.81	7560.81
Initial Force (lbs)	670	670	470	0	350	350
Theoretical ES (psi)	2951.78455	3016.793	1666.53274	0	1247.442	1229.984
Theoretical S (psi)	1858.08538	1858.085	1858.08538	1858.085	1858.085	1858.085
Theoretical ES,S (lbs)	3.074	3.116	2.253	1.188	1.985	1.974
Exp ES, S, & C (in)	0.00575	0.00575	0.00575	0.00575	0.00575	0.00575
Exp ES, S, & C (lbs)	10.47	10.47	10.47	10.47	10.47	10.47
Theo Relaxation (K=10) (lbs)	-42.6022219	-42.60222	-44.919865	0	-40.69673	-40.69673
Exp Relaxation (lbs)	0	0	0	0	0	0
Force Applied (psi)	659.53	659.53	459.53	-10.47	339.53	339.53
Exp MOR (psi)	478.115144	478.1151	718.167454	718.1675	783.5364	783.5364
Theo MOR (psi)	790.726	790.726	993.631	993.631	1043.435	1043.435
Theo MOR (lbs)	193.730637	186.4493	231.428822	241.7047	231.9149	237.6993
L (in)	20.25	19.875	18.75	19	19	18.875
t1 (in)	1.059	1.005	1.002	1.024	1.013	1.0165
t2 (in)	1.027	1.023	1.0245	1.049	0.9805	1.004
t3 (in)	1.029	0.9975	1.0055	1.0225	0.9555	0.983
t4 (in)	1.034	1.0555	1.0205	1.054	1.014	1.0015
b1 (in)	4.097	4.078	4.0805	4.07	4.0675	4.0915
b2 (in)	4.101	4.077	4.0885	4.0675	4.084	4.089
t_ave (in)	1.03725	1.02025	1.013125	1.037375	0.99075	1.00125
b_ave (in)	4.099	4.0775	4.0845	4.06875	4.07575	4.09025
P_computer (lbs)	430.8	414.9	193.3	171.1	169.8	188.4
Crack (lbs)	198.5	153.7	193.3	171.1	169.8	188.4
P load cell (lbs)	430.8	417.2	193.1	172.8	169.8	188.8
Stress (psi)	1758.34218	1769.333	829.067353	710.3685	763.9668	828.7806
Theoretical Crack (lbs)	155.145	150.120	193.134	174.094	192.838	197.379
Actual Crack (lbs)	198.5	156	193.1	172.8	169.8	188.8
Crack Percent Error (%)	-27.94	-3.92	0.02	0.74	11.95	4.35
Ave Percent Error (%)		-15.93		0.38		8.15
Stress Crack (psi)	810.192486	661.5915	829.067353	710.3685	763.9668	828.7806
n (Hz)	346	339	423	428	406	426
W (g)	2961	2801.2	2818	2814.4	2736	2739.4
L (m)	0.51435625	0.504831	0.47625579	0.482606	0.482606	0.479431
t (m)	0.02634647	0.025915	0.02573369	0.02635	0.025165	0.025432
b (m)	0.10411587	0.10357	0.10374756	0.103348	0.103525	0.103894
W (kg)	2.961	2.8012	2.818	2.8144	2.736	2.7394
K (m)	0.00760579	0.007481	0.00742889	0.007607	0.007265	0.007342
K/L	0.01478702	0.014819	0.01559854	0.015762	0.015053	0.015314
T	1.05132954	1.051464	1.05475944	1.055457	1.052448	1.053548
C	71108.4867	71029.33	60990.8908	59383.9	67857.44	64294.45
Dynamic Ec (psi)	3655946.5	3316416	4460407.02	4440480	4438675	4635920
Static Ec (psi)	3034435.6	2752626	3702137.83	3685598	3684101	3847813

Ave Comp (psi)		4341.997		6856.263		7560.81
Ave Break Stress (psi)		1763.838		769.7179		796.3737
Ave Crack Stress (psi)		661.5915		829.0674		828.7806
Ave Dynamic Ec (psi)		3486181		4450443		4537298
Ave Static Ec (psi)		2893531		3693868		3765957

	Straight	
0.075 SMA X	1	2
Comp 2x4 (lbs)	12140	13100
fc' (psi)	3864.282	4169.86
Conv to 4x8 (psi)	6213.882	6876.985
Initial Force (lbs)	741	741
Theoretical ES (psi)	3609.992	3516.495
Theoretical S (psi)	1858.085	1858.085
Theoretical ES,S (lbs)	3.495	3.435
Exp ES, S, & C (in)	0.00575	0.00575
Exp ES, S, & C (lbs)	10.47	10.47
Theo Relaxation (K=10) (lbs)	-44.84879	-44.84879
Exp Relaxation (lbs)	0	0
Force Applied (psi)	730.53	730.53
Exp MOR (psi)	689.098	689.098
Theo MOR (psi)	970.846	970.846
Theo MOR (lbs)	224.673	237.2561
L (in)	20	20
t1 (in)	0.9905	1.0305
t2 (in)	1.0125	1.024
t3 (in)	1.037	1.068
t4 (in)	0.9905	1.0235
b1 (in)	4.099	4.1025
b2 (in)	4.1065	4.0865
t_ave (in)	1.007625	1.0365
b_ave (in)	4.10275	4.0945
P_computer (lbs)	425.7	416.8
Crack (lbs)	200.6	153.7
P load cell (lbs)	422.2	366.1
Stress (psi)	1824.391	1498.072
Theoretical Crack (lbs)	200.365	210.468
Actual Crack (lbs)	197.1	103
Crack Percent Error (%)	1.63	51.06
Ave Percent Error (%)		26.35
Stress Crack (psi)	851.6991	421.4735
n (Hz)	340	324
W (g)	2835.6	2806
L (m)	0.508006	0.508006
t (m)	0.025594	0.026327
b (m)	0.104211	0.104002
W (kg)	2.8356	2.806
K (m)	0.007389	0.0076
K/L	0.014544	0.014961
T	1.050316	1.05206
C	74588.83	68779.23
Dynamic Ec (psi)	3546209	2938480
Static Ec (psi)	2943354	2438939

Ave Comp (psi)		6545.434
Ave Break Stress (psi)		1824.391
Ave Crack Stress (psi)		851.6991
Ave Dynamic Ec (psi)		3242345
Ave Static Ec (psi)		2691146